NAVAL POSTGRADUATE SCHOOL

MONTEREY, CALIFORNIA

THESIS

CROSS-EYE JAMMING AND THE USE OF UAVS AS A CROSS-EYE JAMMER PLATFORM

by

Dimitrios Mastrantonis

June 2021

Thesis Advisor: David C. Jenn
Second Reader: Ric Romero

Approved for public release. Distribution is unlimited.

THIS PAGE INTENTIONALLY LEFT BLANK

REPORT DOCUMENTATION PAGE			Form Approved OMB No. 0704-0188

1. AGENCY USE ONLY *(Leave blank)*	**2. REPORT DATE** June 2021	**3. REPORT TYPE AND DATES COVERED** Master's thesis

4. TITLE AND SUBTITLE CROSS-EYE JAMMING AND THE USE OF UAVS AS A CROSS-EYE JAMMER PLATFORM	**5. FUNDING NUMBERS**
6. AUTHOR(S) Dimitrios Mastrantonis	
7. PERFORMING ORGANIZATION NAME(S) AND ADDRESS(ES) Naval Postgraduate School Monterey, CA 93943-5000	**8. PERFORMING ORGANIZATION REPORT NUMBER**
9. SPONSORING / MONITORING AGENCY NAME(S) AND ADDRESS(ES) N/A	**10. SPONSORING / MONITORING AGENCY REPORT NUMBER**

11. SUPPLEMENTARY NOTES The views expressed in this thesis are those of the author and do not reflect the official policy or position of the Department of Defense or the U.S. Government.

12a. DISTRIBUTION / AVAILABILITY STATEMENT Approved for public release. Distribution is unlimited.	**12b. DISTRIBUTION CODE** A

13. ABSTRACT (maximum 200 words)

Cross-eye jamming is a technique used against monopulse radars. Monopulse radars process the left and right received lobes of the target and use the sum and difference of these lobes to track the target. Cross-eye jamming interferes with the difference signal, and it strives to point the radar beam away from the target. Two jammers, usually at the edges of the target wings, receive a pulse from the radar; they send the pulse from one jammer to the other, and then they transmit the pulse back to the radar, with a phase shift of 180 degrees introduced to one of the two signals. The theory of cross-eye jamming was developed in 1958, and the first cross-eye jammer was established in the late 1970s. However, unmanned aerial vehicles (UAVs) have never been used as transmitters for cross-eye jamming, but they could provide many advantages without the restrictions of distance between them or between the transmitters and the radar. MATLAB software was used to model the jamming environment, and simulations were conducted to investigate the effectiveness of using UAVs.

14. SUBJECT TERMS cross-eye jamming, artificial-glint jamming, UAV, jamming, monopulse RADAR	**15. NUMBER OF PAGES** 69
	16. PRICE CODE

17. SECURITY CLASSIFICATION OF REPORT	**18. SECURITY CLASSIFICATION OF THIS PAGE**	**19. SECURITY CLASSIFICATION OF ABSTRACT**	**20. LIMITATION OF ABSTRACT**
Unclassified	Unclassified	Unclassified	UU

NSN 7540-01-280-5500

Standard Form 298 (Rev. 2-89)
Prescribed by ANSI Std. 239-18

THIS PAGE INTENTIONALLY LEFT BLANK

Approved for public release. Distribution is unlimited.

CROSS-EYE JAMMING AND THE USE OF UAVS AS A CROSS-EYE JAMMER PLATFORM

Dimitrios Mastrantonis
Lieutenant Commander, Hellenic Navy
BNS, Hellenic Naval Academy, 2005

Submitted in partial fulfillment of the
requirements for the degree of

MASTER OF SCIENCE IN ELECTRICAL ENGINEERING

from the

NAVAL POSTGRADUATE SCHOOL
June 2021

Approved by: David C. Jenn
Advisor

Ric Romero
Second Reader

Douglas J. Fouts
Chair, Department of Electrical and Computer Engineering

THIS PAGE INTENTIONALLY LEFT BLANK

ABSTRACT

Cross-eye jamming is a technique used against monopulse radars. Monopulse radars process the left and right received lobes of the target and use the sum and difference of these lobes to track the target. Cross-eye jamming interferes with the difference signal, and it strives to point the radar beam away from the target. Two jammers, usually at the edges of the target wings, receive a pulse from the radar; they send the pulse from one jammer to the other, and then they transmit the pulse back to the radar, with a phase shift of 180 degrees introduced to one of the two signals. The theory of cross-eye jamming was developed in 1958, and the first cross-eye jammer was established in the late 1970s. However, unmanned aerial vehicles (UAVs) have never been used as transmitters for cross-eye jamming, but they could provide many advantages without the restrictions of distance between them or between the transmitters and the radar. MATLAB software was used to model the jamming environment, and simulations were conducted to investigate the effectiveness of using UAVs.

THIS PAGE INTENTIONALLY LEFT BLANK

TABLE OF CONTENTS

LIST OF FIGURES

LIST OF TABLES

THIS PAGE INTENTIONALLY LEFT BLANK

LIST OF ACRONYMS AND ABBREVIATIONS

EA	electronic attack
EP	electronic protection
ES	electronic support
EW	electronic warfare
JSR	jammer-to-signal ratio
LOS	line of sight
RADAR	radio detection and ranging
RCS	radar cross section
UAV	unmanned aerial vehicle

THIS PAGE INTENTIONALLY LEFT BLANK

ACKNOWLEDGMENTS

First of all, I would like to thank the Hellenic Navy for giving me the opportunity to study at the Naval Postgraduate School.

I would like to express my gratitude to my thesis advisor, Professor David C. Jenn, for his patience and guidance over the past year. His guidance helped me tremendously in this thesis. I really appreciate his efforts to go through this thesis with me to ensure its quality, despite his busy schedule. I could not have imagined a better advisor and mentor. Moreover, I would like to thank my second reader, Professor Ric Romero, for spending precious time on my thesis and providing me with his valuable advice.

Also, I would like to thank my family, whom I missed these two years of study, and my daughter, Asimina, who inspires my life. Finally, I would like to express my deepest appreciation and love to my wife, Angeliki Margara, for her support and understanding during my studies at the Naval Postgraduate School.

THIS PAGE INTENTIONALLY LEFT BLANK

I. INTRODUCTION

A. MOTIVATION

In the constant battle between electronic support (ES) and electronic attack (EA) measures, the evolution of technology provides opportunities for both divisions of electronic warfare (EW) to evolve further. A great electronic protect (EP) measure is the highly accurate tracking radar technique called monopulse. Monopulse radars determine the target angle with two simultaneously received signals [1]. Only a few effective jamming techniques against monopulse radars exist, and one of them is cross-eye jamming [2]. Cross-eye jamming is a technique that can deceive a monopulse radar, which emphasizes the significance of this EA method [2], [3]. Specifically, for an airborne application, the cross-eye system typically consists of two connected antennas separated as far apart as possible (e.g., at the wing tips of an aircraft). These antennas receive radar signals and then retransmit the signals to the radar, thereby inducing angle errors in the radar measurements.

The operation of cross-eye jamming is like the physical phenomenon of glint [2]–[5]. Glint induces range and angle errors in the radar tracking because the radar cross section (RCS) of targets, due to its complexity, can vary significantly in amplitude and phase with small angle fluctuations [1], [6], [7]. Cross-eye jamming replicates the error that glint can cause, so it is also called “artificial-glint jamming” [2], [3], [5].

This technique, even though is one of a few jamming techniques effective against monopulse radars, suffers mainly from two limitations [2]. First, narrow margins exist in implementing cross-eye jammers, and the many uncontrollable and unpredictable parameters involved can negate the induced tracking errors, thus making the jamming ineffective [2], [8]. Second, there is a need for a high jammer-to-signal ratio (JSR), which requires high power [2], [8]. Furthermore, for conventional implementation, the position of the antennas is limited by the physical length of the target. The distance between the two antennas plays an important role in the effectiveness of the system, improving the results as the antenna distance increases [3], [4], [9].

Today, unmanned aerial vehicles (UAVs) are used in a large variety of applications, offering safe and low-cost solutions to a wide range of problems. A new era has begun for the military industry, which can fabricate UAVs for several purposes. A straightforward application using UAVs in cross-eye jamming would be to have two UAVs escorting an aircraft. A representative example is the innovative "loyal wingman" of Boeing, shown in Figure 1. This project of Boeing involves the use of UAVs that escort and protect high-value platforms. Exploiting this new technology, UAVs can be used as cross-eye jammer platforms, overcoming many of the limitations of the cross-eye jamming technique. Specifically, the antennas can be placed anywhere, causing the greatest angle error to the radar with less power needed.

Figure 1. "Loyal Wingman" escort an aircraft. Source: [10].

B. BACKGROUND

First, the operation of a monopulse radar is briefly described in this section to illustrate the operation of cross-eye jamming. As shown in Figure 2, the radar antenna is

pointed at the target and receives the return signal (echo) from the target [1], [6]. The radar antenna has sum and difference beams, as shown in Figure 2 [6]. When receiving, the ratio of the difference beam output to sum beam output results in the error signal shown in Figure 3 [1], [3], [11]. If the antenna is on target, the error signal is zero because the difference beam null is on the target. If the antenna is not on target, the radar uses the negative or positive voltage of the error signal to apply a correction angle and moves the direction of the antenna beam toward the target [1], [6].

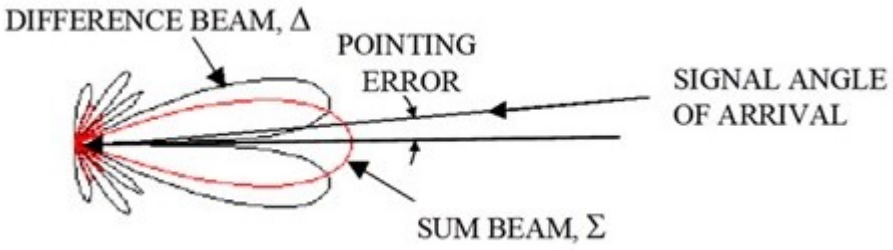

Figure 2. Sum (red) and difference (black) beams of a monopulse radar with a pointing error

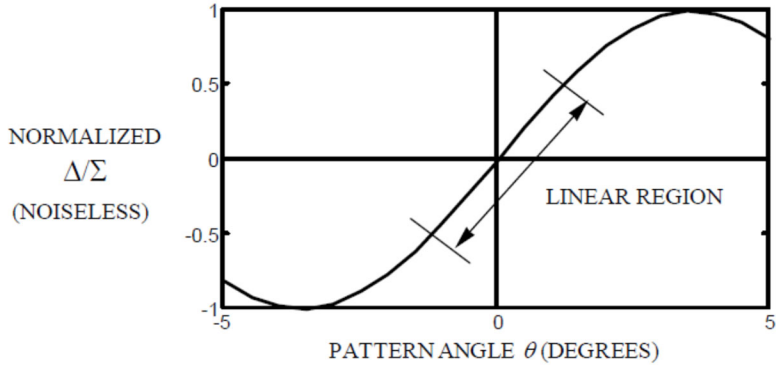

Figure 3. Error signal of a monopulse radar with a linear region. Source: [12].

The objective of cross-eye jamming is to induce an angle error in a monopulse radar and cause it to lose tracking of the target [2], [3], [9], [11]. The cross-eye jammer is a system of two antennas, usually positioned at the edges of the aircraft wings, as shown in

Figure 4. Each antenna receives and retransmits the signal from the radar. The two signals in the difference beam output have almost matched amplitudes and a phase difference of approximately 180° [2], [4], [11]. The radar receives the two signals that combine and give an erroneous voltage error in the difference beam output, causing the antenna to point away from the target. The only way to construct an operating cross-eye jammer seems to be the retrodirective implementation, as shown in Figure 5 [4]. The two jammer antennas receive a pulse from the radar [4]. Then, each antenna sends the pulse to the other, although one of the two signals is changed in amplitude and phase relative to the other (the amplitude is approximately matched and the phase is shifted roughly 180°) [4], [11]. Finally, the two signals are retransmitted back to the radar, where they combine with the radar echo from the target [4], [11].

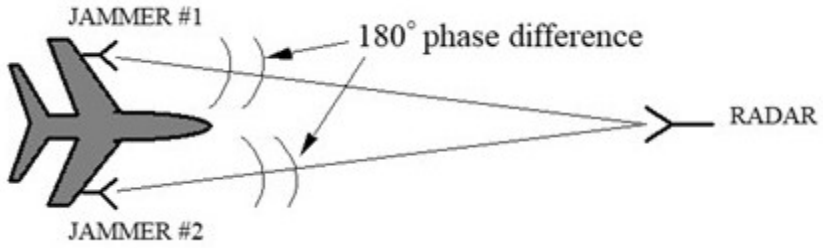

Figure 4. An example of an aircraft with cross-eye jammers

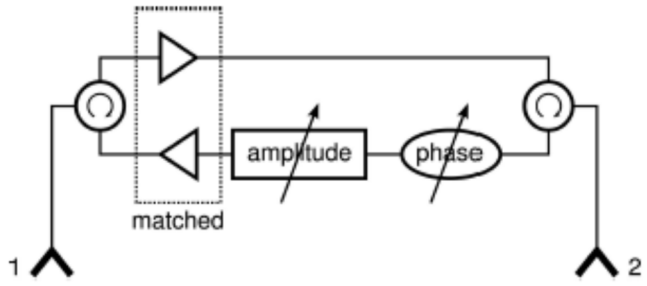

Figure 5. A cross-eye jammer implemented in a retrodirective way. Source: [4].

The theory of cross-eye jamming was developed in 1958, and the first cross-eye jammer was created in the late 1970s [2]. However, the first operational cross-eye jammers

were only constructed within the last two decades, confirming the difficulty of implementing the technique [13]. Nevertheless, the evolution in electronics has made the implementation of an operational cross-eye jammer feasible [13].

Most studies have used glint analyses to examine cross-eye jamming, as both are based on the same physical principles [3], [14], [15]. In glint analyses, it is assumed that the target surfaces form the transmitter, and the radar the receiver [3]. Moreover, the target surfaces are supposed to be at the same distance from the radar (referred to as a point target), and to compensate for the different distances, an amplitude and a phase difference are introduced for each surface [3]. However, this approach ignores the retrodirective implementation of cross-eye jamming and has led to erroneous conclusions concerning the effectiveness of the cross-eye jamming technique [3], [9].

C. PREVIOUS RESEARCH

A short historical review of glint and cross-eye jamming analyses is given here. To begin with, in 1953, Delano discovered that glint could cause angle errors in radar tracking, which later led to the invention of cross-eye jamming [16].

Linear fit analysis was introduced by Meade [17]; Sherman in 1970 [18] and, later, Schleher [19] used linear fit analysis for monopulse radars, as did Vakin and Shustov [20]. In linear fit analysis, the indicated angle is calculated using linear fits of the sum and difference signals of a radar to get the difference-over-sum ratio shown in Figure 3 [18], [20]. Fit analysis is important because it shows that cross-eye jamming does not induce a constant angle error but an increasing error as the distance closes [3], [21].

Another type of analysis is phase front analysis, which was introduced by Howard and Lewis, as mentioned in [3]. The concept of this analysis is that the radar seeks maximum power in the direction of the return signal phase front direction [3], [15]. Lindsay as well as Dunn and Howard went a step further and used the derivative of the signal phase front to explain the angle error caused by the phase front distortion [22], [23]. Moreover, Dunn and Howard introduced Poynting vector analysis, which also validated that a complex target could cause angular errors to a radar [23].

Leonov and Fomichev examined glint and cross-eye jamming through phase-comparison monopulse analysis [24]. This analysis showed that both amplitude and phase-comparison monopulse radars are affected by cross-eye jamming [24]. In the late 2000s, a graphical analysis was introduced by Falk [13]. He investigated the angle error by examining received signal vectors of the antenna elements [13]. In the last decade, du Plessis performed a thorough study of retrodirective cross-eye jamming in [2]–[4], [9], providing more accurate results and some new conclusions about this jamming technique. These results showed that cross-eye jamming is more efficient than the previous studies had shown [3].

Many new studies have been conducted over the past two decades trying to overcome the drawbacks of cross-eye jamming. A rotating cross-eye jammer was proposed in [15] to eliminate the effect of the angle of the target with respect to the line between the radar and the target (the line of sight [LOS] of the target). Another proposal has been to use multiple elements instead of two, which has led to better results [5], [14]. Lastly, du Plessis has proposed a variation in the implementation of a retrodirective cross-eye jammer that can affect both the difference and the sum signals of the radar [25].

D. OBJECTIVE

This thesis presents a comprehensive theoretical model of cross-eye jamming that was developed and implemented in MATLAB. A phased array monopulse radar, a target, and a two-element retrodirective cross-eye jammer were modeled, including all of their interactions. The positions of the jammers were not constrained to be on the target, as in all the previous studies. Two UAVs were used as platforms of the cross-eye jammer antennas, as shown in Figure 6. A comprehensive theory was developed, and the governing equations were derived. The equations removed many of the limitations of previously published approaches. Furthermore, wireless or hardwired links between the two jammer antennas were modeled.

This thesis investigates under which circumstances this new approach of using UAVs as jammers is feasible and effective. The use of separate platforms (i.e., UAVs) as jammers opens up a wide range of operational scenarios. When jammers operate close to

the radar, the power requirements are relaxed. Also, due to the low RCS of the UAVs, their detection is very difficult.

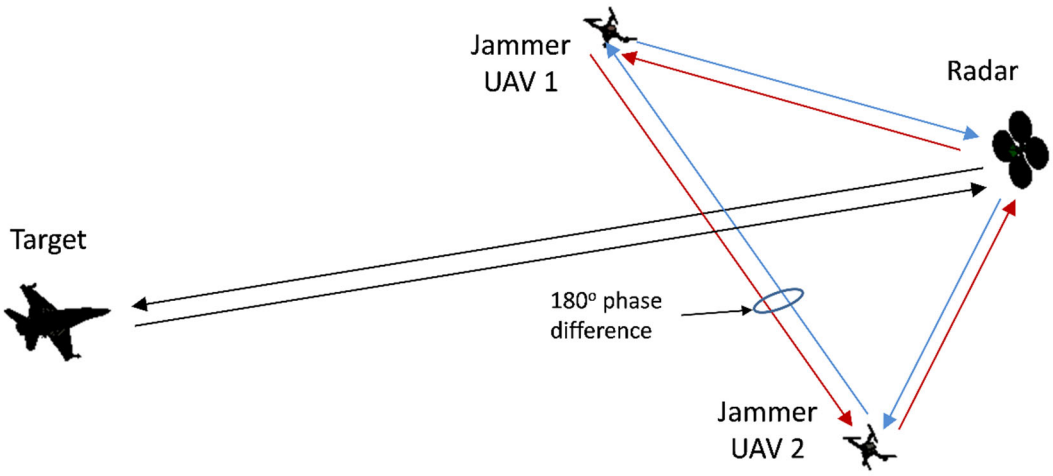

Figure 6. A target accompanied by two UAVs used as cross-eye jammer platforms

A wide separation between antennas results in large errors at the radar. However, the wireless links required for the UAVs introduce time delays and attenuation of the relayed signals. All of these effects could be included in the model. Furthermore, arbitrary radar antennas could be modeled, with low sidelobe patterns on both the sum and difference beams. There were no restrictions or limitations on the formulas other than the UAVs and target had to be in the far field of the radar antenna.

E. THESIS OUTLINE

Chapter II provides the theory and mathematical model of the simulations. The expressions for the difference-over-sum ratio and target angle error are derived. The differences between the wired and wireless implementations are discussed. Simulations were performed, and their outcomes are presented in Chapter III. Finally, Chapter IV presents the conclusion and a brief discussion on the practical implementation using UAVs,

such as power, hardware requirements, and synchronization. This chapter also has suggestions for future work.

II. THEORY AND MODELING

A. INTRODUCTION

This chapter models the components of the simulations: a monopulse radar, a target, and two UAVs forming a retrodirective cross-eye jammer (see Figure 7). We also use a conventional retrodirective cross-eye jammer on the edges of the target wings for comparison between the traditional method (wired connection of the antennas) and the proposed method of UAVs (wireless connection of the antennas). The received electric field due to each component is calculated separately, allowing us to examine the effect of the jammer and the difference between the wired and the wireless case.

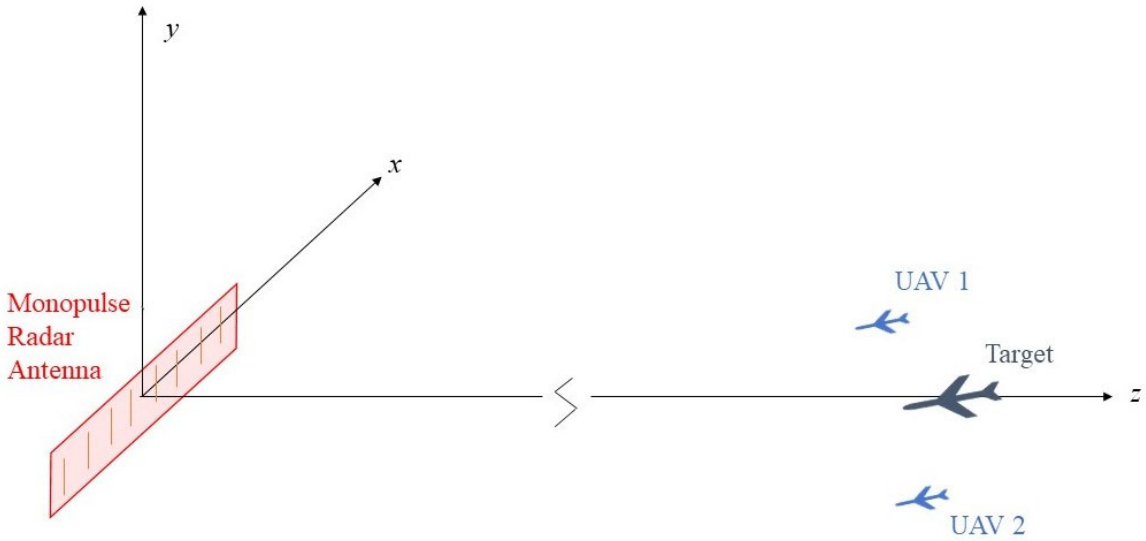

Figure 7. The cross-eye jammer scenario being considered with the use of 2 UAVs

B. SIMULATION ENVIRONMENT

The environment of the simulations and the coordinate system are described in this section. The medium is free space, and no other propagation phenomena, such as sea clutter or surface reflections, are included. Consequently, the only loss considered is spherical dispersion. Also, the receiver noise is ignored, and only the received power for a continuous

wave signal is computed. The coordinate system is defined in Figure 8. The simulations are limited to the azimuth plane (φ=0°) and $-90° \le \theta \le 90°$, as shown in Figure 8. This does not limit the results, as a monopulse radar uses two difference beam nulls to track the target—one for elevation and one for azimuth—and they are processed separately.

First, we define the distances and angles for the target and jammer components in the Cartesian and the spherical coordinate systems. Since the positions are generally given in spherical coordinates, the transformation to cartesian coordinates is as follows:

$$x = R \sin\theta \cos\varphi \tag{2.1}$$

$$y = R \sin\theta \sin\varphi \tag{2.2}$$

$$z = R \cos\theta, \tag{2.3}$$

where (x, y, z) are the cartesian coordinates and (R, θ, φ) are the spherical coordinates. As noted previously, φ=0°, so the radar and jammers are in the azimuth plane for all cases considered; however, this is not a restriction imposed in deriving the equations. In the φ=0° plane (Elevation 0°), θ becomes the azimuth angle, as shown in Figure 8.

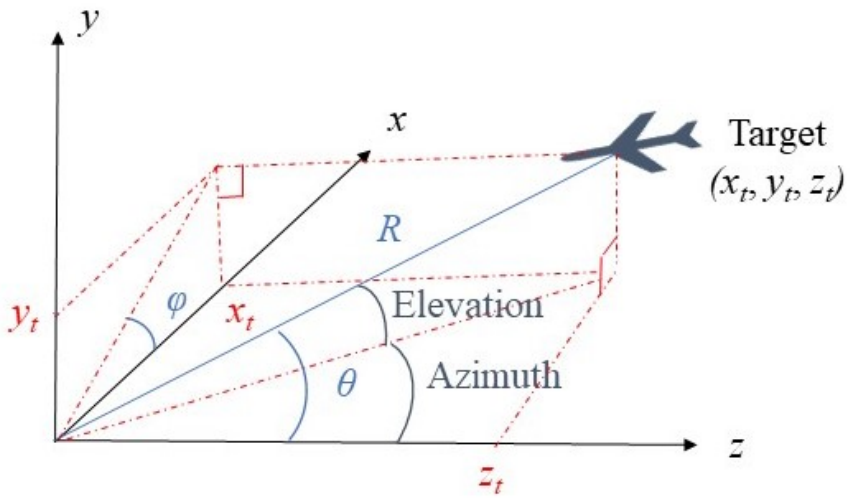

Figure 8. The cartesian (red) and spherical (blue) coordinates

The calculation of distance between two arbitrary points denoted by indices m and n is as follows:

$$R_{mn} = \sqrt{(x_n - x_m)^2 + (y_n - y_m)^2 + (z_n - z_m)^2}\,, \tag{2.4}$$

where (x_m, y_m, z_m) are the cartesian coordinates of point m, and (x_n, y_n, z_n) are the cartesian coordinates of point n. R_{mn} is the distance between them.

C. TARGET AND CROSS-EYE JAMMERS

The cross-eye jammer antennas are omnidirectional in azimuth with gain G_{aj}. Each antenna receives the transmitted signal from the radar and sends it to the other. A cross-eye gain with magnitude α_j and phase φ_j is introduced in one of the two jammer signals whereas both signals are amplified with a gain G_j. Moreover, the distance between the two antennas (referred to as the baseline) is represented as d_c, and the angle of the baseline perpendicular is θ_c, as illustrated in Figure 9.

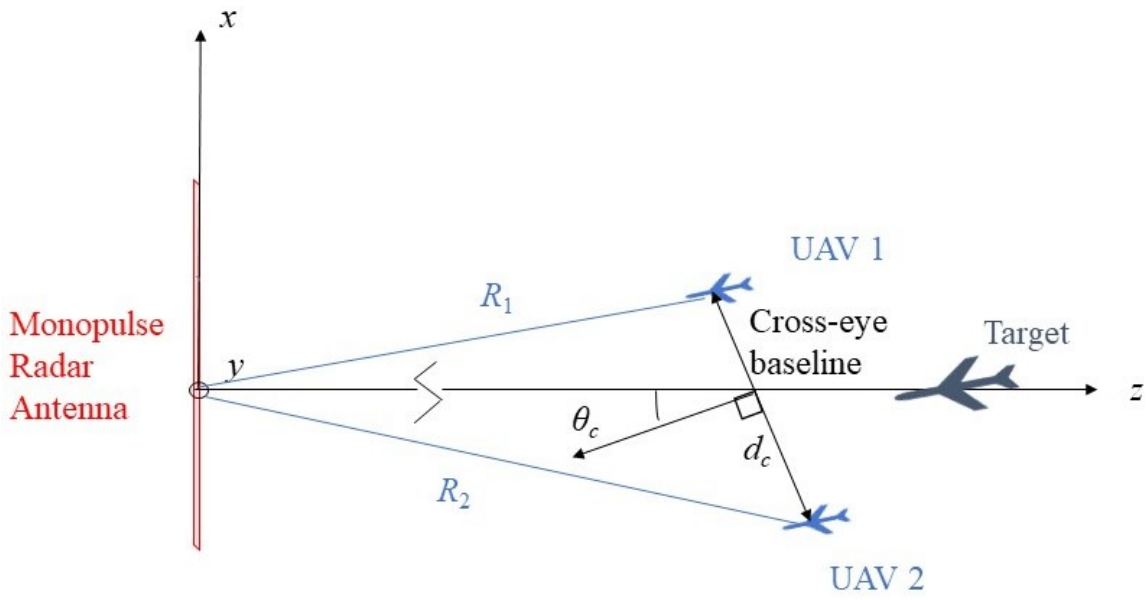

Figure 9. Top view of the target and UAVs with distance d_c and angle θ_c

The distances R_t, R_1, and R_2 are measured from the center of the antenna to the target, to the first UAV and to the second UAV, respectively. Accordingly, θ_t, θ_1, and θ_2 are the angles from the z-axis and the target, the first UAV, and the second UAV, respectively. Furthermore, φ_t, φ_1, φ_2 are the angles of the target, the first UAV, and the second UAV, respectively, projected on the x-y plane (all are 0° as previously noted). All of these values for the target and UAVs are summarized in Tables 1 and 2.

Table 1. Summary of target parameters

Parameter	Symbol and value
Range (m)	R_t
Direction (degrees)	θ_t, $\varphi_t = 0$
RCS (m^2)	$\sigma \cdot e^{j\phi_\sigma}$

Table 2. Summary of jammer parameters

Parameter		Symbol and value
UAV antenna 1	Range (m)	R_1
	Angle (degrees)	θ_1, $\varphi_1 = 0$
UAV antenna 2	Range (m)	R_2
	Angle (degrees)	θ_2, $\varphi_2 = 0$
Cross-eye weight		$\alpha_j e^{j\phi_j}$
Antenna gain (dB)		G_{aj}
Amplifier gain (dB)		G_j
Baseline distance (m)		d_c
Rotation angle (degrees)		θ_c

D. MONOPULSE RADAR

A phased array is used as a monopulse radar antenna. It is a linear array of N elements, which can be designed to model a large variety of antenna types. In the following simulations, the linear array consists of 10 half-wave dipoles aligned with the y-axis and spaced at distance d_x, which is also equal to a half wavelength, as shown in Figure 10.

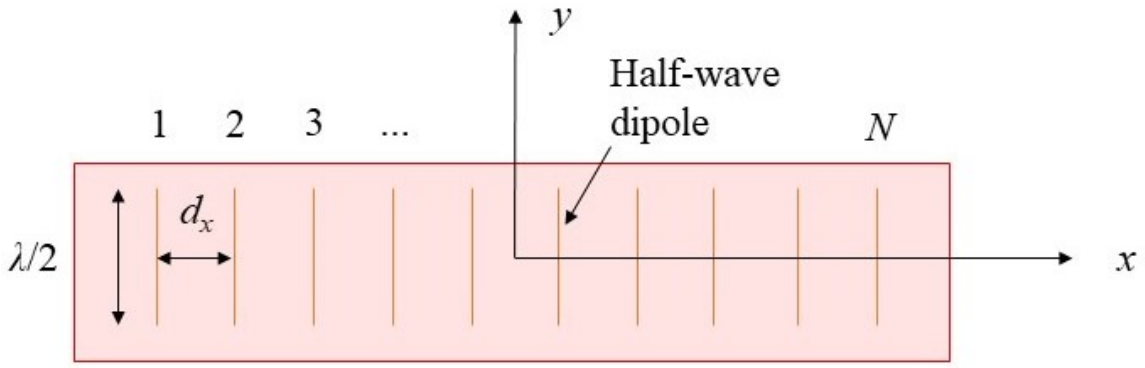

Figure 10. Linear array parameters

Moreover, R_{melt}, R_{mel1}, and R_{mel2} are the distances between array element m and the target, the first jammer antenna, and the second, respectively. To be more realistic, a plate behind the dipoles has been modeled to improve the performance and provide a hemispherical pattern. For convenience, the default frequency used is 300 MHz unless otherwise noted. The mutual coupling of the elements is ignored. When transmitting, the elements are fed by a Taylor amplitude taper A_{tsxm} and an appropriate element phase difference to point the beam at the target. On the other hand, when the radar acts as the receiver, the Taylor sum beam is used along with the difference beam, which has a Bayliss distribution with a sidelobe taper A_{tdxm}. The relative difference between the main beam peak and the sidelobes is generally set to 20 dB.

The antenna pattern direction (field point) is (θ, φ). The antenna main beam scan direction is (θ_s, φ_s). We define the direction cosines u, u_s, v, and v_s as follows:

$$u = \sin\theta\cos\varphi \tag{2.5}$$

$$u_s = \sin\theta_s \cos\varphi_s \tag{2.6}$$

$$v = \sin\theta \sin\varphi \tag{2.7}$$

$$v_s = \sin\theta_s \sin\varphi_s \,. \tag{2.8}$$

The element m phase to scan the beam is

$$\Delta\Phi_m = e^{jm\beta(u-u_s)} e^{j\beta(v-v_s)}, \tag{2.9}$$

where $m = 1, 2, \ldots, N$, and $\beta = 2\pi/\lambda$ is the wavenumber. An element factor can be specified for the array. The element factor for half-wavelength dipoles aligned with the y-axis is

$$\left|EF\right| = \left| \frac{\cos\left(\frac{\pi}{2} v\right)}{\sqrt{u^2 + \cos^2\theta}} \right| \quad \left(-90° \le \theta \le 90°\right). \tag{2.10}$$

For the sum beam, the electric field in the direction (θ, φ) or (u, v) is [26]:

$$\left|E_s\right| = \left| \sum_{m=1}^{N} A_{tsxm} e^{jm\beta(u-u_s)} e^{j\beta(v-v_s)} \left|\cos\theta\right| \left|EF_m\right| \right|. \tag{2.11}$$

The sum beam solid angle is derived from [26]:

$$\Omega_s = \int_0^{2\pi} \int_0^{\pi/2} \left|E_{snorm}\right|^2 \sin\theta d\theta d\varphi \,, \tag{2.12}$$

where E_{snorm} is

$$\left|E_{snorm}\right| = \frac{\left|E_s\right|}{\left|E_{s\max}\right|}, \tag{2.13}$$

and $E_{s\max}$ is the maximum value of the electric field. Since the beam solid angle is calculated in Equation 2.12, the gain of the sum beam can be determined by [26]:

$$G_s = \frac{4\pi \left| E_{snorm} \right|^2}{\Omega_s}. \tag{2.14}$$

For the difference beam, half of the array elements are multiplied by -1. This is accomplished by an extra factor e^{jfazm}, where *fazm* is equal to π for the first half of the elements and zero for the rest. The electric field is

$$\left| E_d \right| = \left| \sum_{m=1}^{N} A_{tdxm} e^{jm\beta(u-u_s)} e^{j\beta(v-v_s)} e^{jfazm} \left| \cos\theta_s \right| \left| EF_m \right| \right|. \tag{2.15}$$

The difference beam solid angle is

$$\Omega_d = \int_0^{2\pi} \int_0^{\pi/2} \left| E_{dnorm} \right|^2 \sin\theta d\theta d\varphi, \tag{2.16}$$

where E_{dnorm} is

$$\left| E_{dnorm} \right| = \frac{\left| E_d \right|}{\left| E_{d\max} \right|}, \tag{2.17}$$

and $E_{d\max}$ is the maximum value of the electric field. Similarly, the gain of the difference beam is

$$G_d = \frac{4\pi \left| E_{dnorm} \right|^2}{\Omega_d}. \tag{2.18}$$

We note that if the field point is far from the array, then the element factor of all elements is the same, $\left| EF_m \right| = \left| EF \right|$. The condition for this is that $R > 2(Nd)^2 / \lambda$, which is met in almost all practical situations. The radar parameters are summarized in Table 3.

Table 3. Summary of radar parameters

Parameter	Symbol and value
Transmit power (W)	$P_t = 1$
Frequency (MHz)	$f = 300$
Sum beam gain (dB)	G_s
Sum beam relative sidelobe level (dB)	$sll_s = 20$
Difference beam gain (dB)	G_d
Difference beam relative sidelobe level (dB)	$sll_d = 20$
Number of elements	$N = 10$
Spacing between elements (m)	$d_x = 0.5$

E. RECEIVED TARGET AND JAMMER SIGNALS

After defining all the necessary parameters, the electric fields can be calculated. The electric fields at the target and UAVs are as follows:

$$E_{it} = \frac{\sqrt{60 \cdot P_t \cdot G_s}}{E_{ms}} \sum_{m=1}^{N} \frac{A_{tsxm} e^{-j\beta m u_s} e^{-j\beta v_s} e^{-j\beta R_{melt}} EF_m}{R_{melt}} \tag{2.19}$$

$$E_{ijam1} = \frac{\sqrt{60 \cdot P_t \cdot G_s}}{E_{ms}} \sum_{m=1}^{N} \frac{A_{tsxm} e^{-j\beta m u_1} e^{-j\beta v_1} e^{-j\beta R_{mel1}} EF_m}{R_{mel1}} \tag{2.20}$$

$$E_{ijam2} = \frac{\sqrt{60 \cdot P_t \cdot G_s}}{E_{ms}} \sum_{m=1}^{N} \frac{A_{tsxm} e^{-j\beta m u_2} e^{-j\beta v_2} e^{-j\beta R_{mel2}} EF_m}{R_{mel2}}. \tag{2.21}$$

P_t is the transmitted power of the radar, u_1 and v_1 give the direction of the first jammer, u_2 and v_2 give the direction of the second jammer, and EF_m is the element factor.

Since each jammer antenna sends its received signal to the other, the signal transmitted back to the radar from each jammer when there is a hardwired connection between them is as follows:

$$E_{tjam12} = E_{ijam1} \frac{G_{aj}\lambda}{(4\pi)} \sqrt{G_j} \tag{2.22}$$

$$E_{tjam21} = E_{ijam2} \frac{G_{aj}\lambda}{(4\pi)} \alpha_j e^{j\varphi_j} \sqrt{G_j} \ . \tag{2.23}$$

As defined here, there is no loss in the wired connection, although it could easily be added. For the wireless case,

$$E_{tjam12} = E_{ijam1} \frac{G_{aj}^2\lambda^2}{(4\pi)^2} \frac{e^{-j\beta d_c}}{d_c} \sqrt{G_j} \tag{2.24}$$

$$E_{tjam21} = E_{ijam2} \frac{G_{aj}^2\lambda^2}{(4\pi)^2} \frac{e^{-j\beta d_c}}{d_c} \alpha_j e^{j\varphi_j} \sqrt{G_j} \ . \tag{2.25}$$

Finally, at the radar, the received signals from the target and the jammers for the sum beam are

$$E_{rst} = E_{it} \sqrt{\frac{\sigma_t G_s \lambda^2}{E_{ms}^2 (4\pi)^2} \frac{1}{2\eta_0}} \sum_{m=1}^{N} \frac{A_{txsm} e^{-j\beta m u_s} e^{-j\beta v_s} e^{-j\beta R_{melt}} EF_m}{R_{melt}} \tag{2.26}$$

$$E_{rsjam1} = E_{tjam21} \sqrt{\frac{G_s \lambda^2}{E_{ms}^2 (4\pi)^2} \frac{1}{2\eta_0}} \sum_{m=1}^{N} \frac{A_{tsxm} e^{-j\beta m u_1} e^{-j\beta v_1} e^{-j\beta R_{mel1}} EF_m}{R_{mel1}} \tag{2.27}$$

$$E_{rsjam2} = E_{tjam12} \sqrt{\frac{G_s \lambda^2}{E_{ms}^2 (4\pi)^2} \frac{1}{2\eta_0}} \sum_{m=1}^{N} \frac{A_{tsxm} e^{-j\beta m u_2} e^{-j\beta v_2} e^{-j\beta R_{mel2}} EF_m}{R_{mel2}} \tag{2.28}$$

and for the difference beam are

$$E_{rdt} = E_{it} \sqrt{\frac{\sigma_t G_d \lambda^2}{E_{md}^2 (4\pi)^2} \frac{1}{2\eta_0}} \sum_{m=1}^{N} \frac{A_{tdxm} e^{-j\beta m u_s} e^{-j\beta v_s} e^{-j\beta R_{melt}} EF_m}{R_{melt}} \tag{2.29}$$

$$E_{rdjam1} = E_{tjam21}\sqrt{\frac{G_d\lambda^2}{E_{md}^2(4\pi)^2}\frac{1}{2\eta_0}}\sum_{m=1}^{N}\frac{A_{tdxm}e^{-j\beta mu_1}e^{-j\beta v_1}e^{-j\beta R_{mel1}}EF_m}{R_{mel1}} \quad (2.30)$$

$$E_{rdjam2} = E_{tjam12}\sqrt{\frac{G_d\lambda^2}{E_{md}^2(4\pi)^2}\frac{1}{2\eta_0}}\sum_{m=1}^{N}\frac{A_{tdxm}e^{-j\beta mu_2}e^{-j\beta v_2}e^{-j\beta R_{mel2}}EF_m}{R_{mel2}}. \quad (2.31)$$

σ_t is the complex RCS of the target, and η_0 is the intrinsic impedance of air.

With the set of Equations 2.25–2.30, the received electric field due to each component is determined. An example is presented for further understanding. For this example, a target with the conventional cross-eye jammer (wired connection between the jammer antennas) is used. The values of the parameters are as follows: R_t = 1000 m, θ_t = 0°, σ = 1 m^2, φ_σ = 0°, d_c = 10 m, θ_c = 0°, α_j = -0.5 dB, φ_j = 175°, G_{aj} = 1.64, G_j = 40 dB. The remaining values are listed in Tables 1–3. The transmitted sum and difference fields at the target are illustrated in Figure 11. The designed sidelobes are 20 dB lower than the main beam peak.

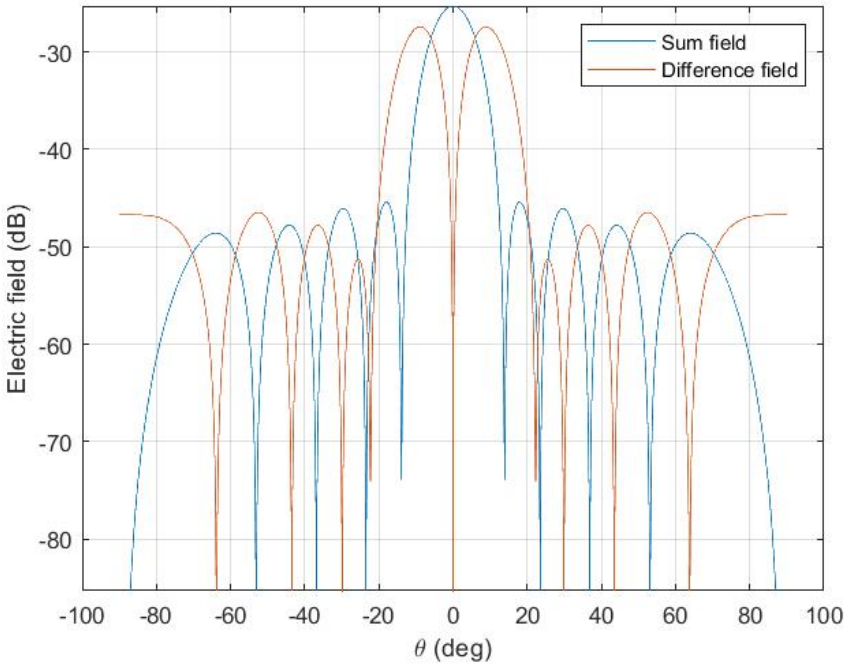

Figure 11. Transmitted sum and difference fields at the range of the target, 1,000 m

The received sum and difference fields from the target only are illustrated in Figure 12 and from the target with the jammer operating in Figure 13. The distortion of the difference beam pattern is evident. In Figure 12, the sidelobes of the sum field are 40 dB lower than the main beam whereas the sidelobes of the difference field are about 30 dB lower than the main beam. Combining Equation 2.17 with Equation 2.24 (for sum) or 2.27 (for difference) yields the Taylor amplitude taper (when transmitting) with the Taylor amplitude taper (when receiving for the sum beam) or with the Bayliss amplitude taper (when receiving for the difference beam). These products are called “round trip” or “two way” patterns. This explains the lower sidelobes for the sum channel compared to the difference channel.

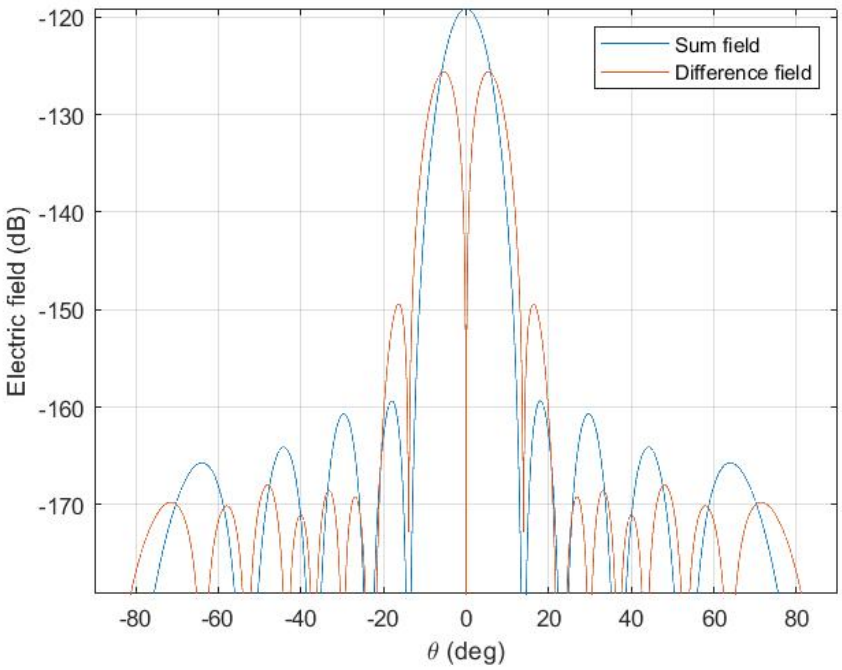

Figure 12. Received sum and difference fields of the target only

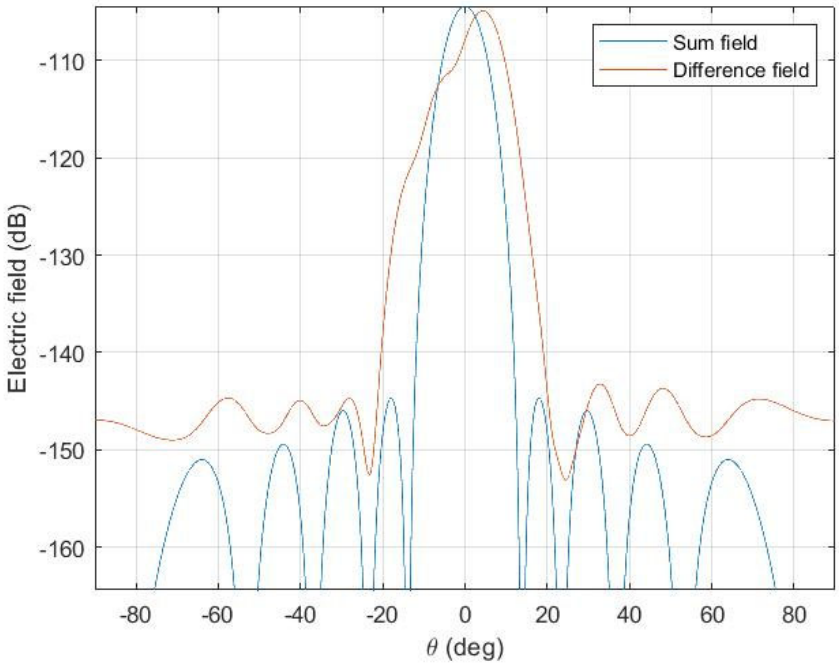

Figure 13. Received sum and difference beams of the target and jammer

The imaginary part of the ratio of the difference channel over the sum channel is illustrated in Figure 14 for the cases with and without a jammer. The steep changes in the curves near $\pm 13°$ are due to the angles approaching the nulls at the edges of the main beam.

A linear fit to the transmitted difference beam over the transmitted sum beam ratio is calculated. This linear fit is applied to the imaginary part of the received difference-over-sum ratio to produce the indicated angle. The indicated angle for this example is shown in Figure 15. The indicated angle error induced by the jammer is approximately 3° even though the sum beam is actually pointed at the target.

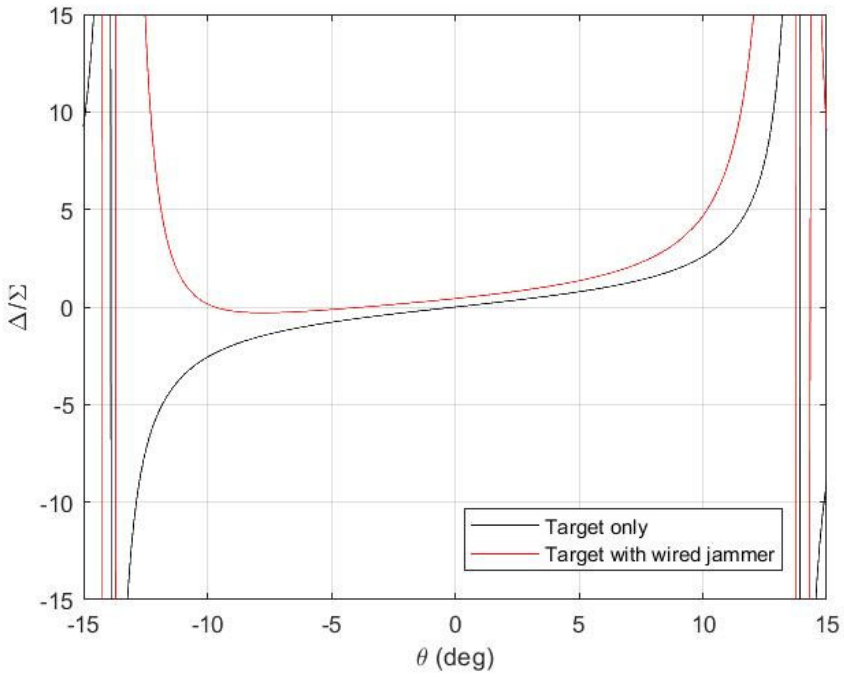

Figure 14. The normalized difference-over-sum ratio of the received signal from the target only and from the target and jammer

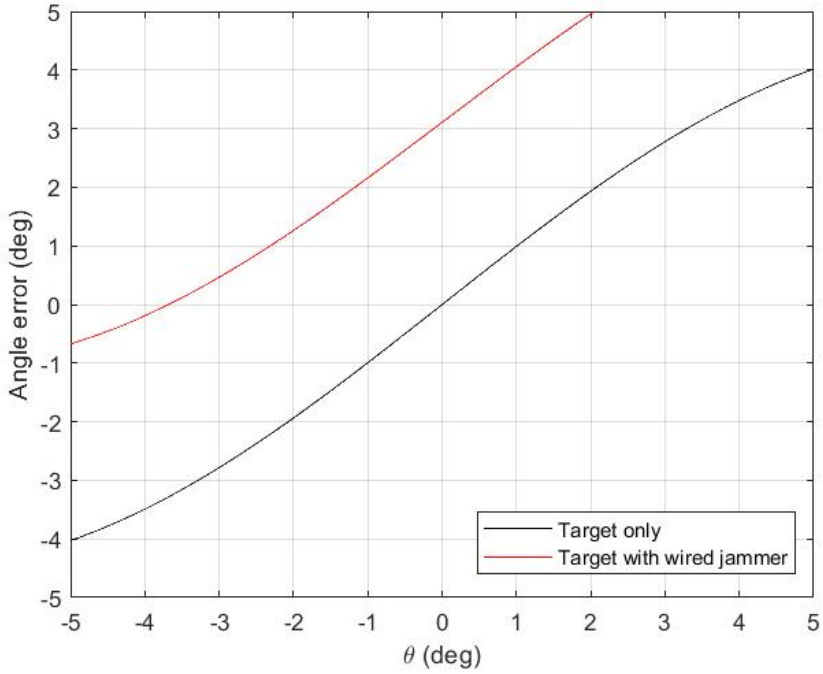

Figure 15. The angle error of the target only and of the target and jammer

F. POWER DIFFERENCE BETWEEN WIRED AND WIRELESS ANTENNAS

Implementing the retrodirective cross-eye technique with UAVs requires the wireless transfer of signals between them. The free space transmission introduces additional loss compared to the hardwired case. If Equations 2.20 and 2.22 are compared, the conclusion drawn is the existence of an extra factor for the power of the wireless jammer relative to a hardwired jammer:

$$\frac{G_{aj}^2 \lambda^2}{(4\pi)^2 d_c^2}. \tag{2.32}$$

Since the antennas of the jammer are omnidirectional, the gain G_{aj} is close to unity (for half-wavelength dipoles, it is 1.64), and the dominant variable is the distance between the antennas d_c. For example, if d_c = 10 m, λ = 1 m, G_{aj} = 1.64, the wireless power is 37.69 dB less than the wired jammer that has no losses. To compensate for this power loss, the antennas must have a larger gain, the UAVs should employ amplifiers, or the jammer should operate close to the radar. Consequently, the distance between the antennas of a

wireless jammer gives rise to power reduction because of the retransmission; however, the larger possible separation increases cross-eye effectiveness, which is desirable.

G. CHAPTER SUMMARY

In this chapter, all of the needed equations for the simulation task were given. We should mention that the parameter values assigned in the beginning of the chapter do not constrain the model. The equations are quite general and could easily be modified and extended to cover other cases as well. In the equations, arbitrary positions of the target and jammer are accounted for. Moreover, it is easy to modify the antenna for a different number of elements, different element types, or a planar instead of a linear array. Finally, some monopulse radars use two difference beams, one for the azimuth and one for the elevation. Only azimuth tracking was modeled here, but it is a simple extension to add an elevation tracking loop.

THIS PAGE INTENTIONALLY LEFT BLANK

III. SIMULATIONS AND RESULTS

This chapter presents various simulations regarding the efficiency of cross-eye jamming in general and the effectiveness of using UAVs as jammer platforms, while various parameters were changed. The chapter is divided into three parts. The first describes the simulations to validate the MATLAB script with published data. The second details the simulations concerning cross-eye jamming in general. In this part, both the classical implementation (hardwired) and the use of UAVs (wireless) are examined. The wireless case is covered in the third part and illustrates the advantages of exploiting UAVs to improve cross-eye performance.

A. VALIDATION SIMULATIONS

Simulations were performed in MATLAB to validate the analytical model presented in Chapter II. The model was modified to replicate the monopulse antenna used in [3], [9]. In these references, the difference beam was formed by subtracting two squinted beams, whereas our model used an array with half the elements phase-shifted 180°, as described in Chapter II. The array parameters were adjusted to give the same patterns, and the remaining parameters were also changed to match those in [3], [9]; the parameters are listed in Table 4.

Table 4. Simulation 1 parameters

Radar		
Parameter		Symbol and value
Transmit power (W)		$P_t = 1$
Frequency (GHz)		$f = 10$
Sum beam gain (dB)		$G_s = 10.54$
Difference beam gain (dB)		$G_d = 10.67$
Difference beam squint angle (degrees)		$\theta_{s1} = 4.5$
Number of elements		$N = 2$
Spacing between elements (m)		$d_x = 0.07616$
Target		
Parameter		Symbol and value
Range (m)		$R_t = 1000$
Direction (degrees)		$\theta_t = 0$, $\varphi_t = 0$
RCS (m^2)		$\sigma \cdot e^{j\phi_\sigma} = 1$
Jammer		
Parameter		Symbol and value
Cross-eye weight (dB, degrees)		$\alpha_j e^{j\phi_j}$, a_j = -0.5, φ_j = 165, 175, 179
Antenna gain (dB)		$G_{aj} = 6$
Amplifier gain (dB)		$G_j = 70$
Baseline distance (m)		$d_c = 10$
Rotation angle (degrees)		$\theta_c = 30$
Antenna 1	Range (m)	$R_1 = 1002.5$
	Angle (degrees)	$\theta_1 = 0.2481$, $\varphi_1 = 0$
Antenna 2	Range (m)	$R_2 = 997.5$
	Angle (degrees)	$\theta_2 = -0.2481$, $\varphi_2 = 0$

The results shown in Figure 16 are similar to the results of [9]. The angle errors for the three different cases (φ_j = 165°, 175°, 179°) are close to the angle errors in [9]. The plots are similar until the indicated angle exceeds ±11°. Results near the main beam nulls vary widely because the sum beam approaches zero and the Δ/Σ ratio is singular.

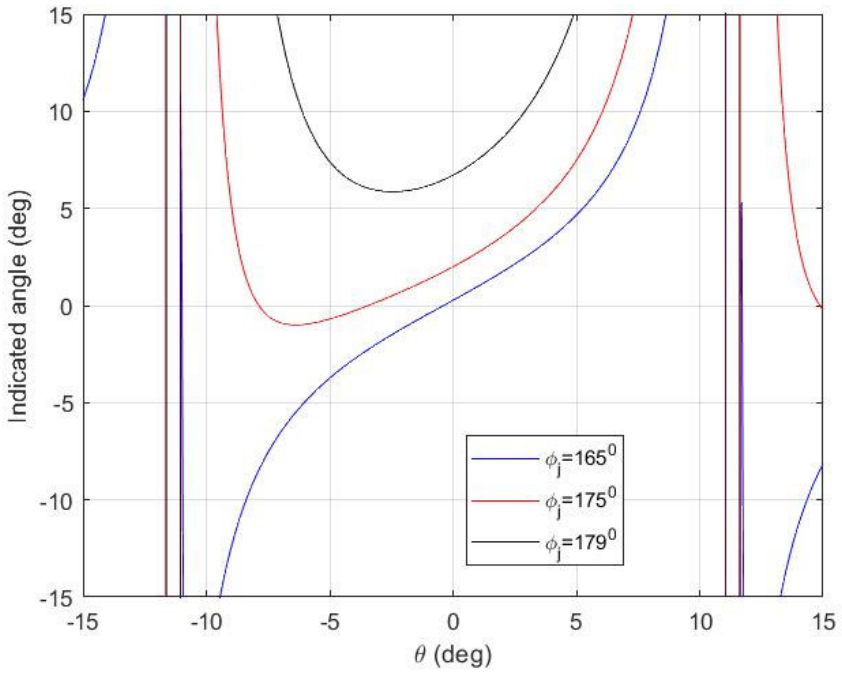

Figure 16. Indicated angles for three different φ_j using the same parameters as [9]

For the rest of the simulations, the parameters of the monopulse radar were those described in Table 3. Another simulation was conducted with the same radar parameters as in Table 3 and the rest of the parameters from Simulation 1. The parameter values are shown in Table 5 and the results in Figure 17. Figures 16 and 17 are similar, indicating that the different radar antenna (but with almost the same beamwidth) and frequency do not affect the results drastically. A summary of results for the two simulations is given in Table 6.

Table 5. Simulation 2 parameters

Radar		
Parameter		Symbol and value
Transmit power (W)		$P_t = 1$
Frequency (MHz)		$f = 300$
Sum beam gain (dB)		$G_s = 10.545$
Sum beam relative sidelobe level (dB)		$sll_s = 20$
Difference beam gain (dB)		$G_d = 10.5$
Difference beam relative sidelobe level (dB)		$sll_d = 20$
Number of elements		$N = 10$
Spacing between elements (m)		$d_x = 0.5$
Target		
Parameter		Symbol and value
Range (m)		$R_t = 1000$
Direction (degrees)		$\theta_t = 0$, $\varphi_t = 0$
RCS (m^2)		$\sigma \cdot e^{j\phi_\sigma} = 1$
Jammer		
Parameter		Symbol and value
Cross-eye weight (dB, degrees)		$\alpha_j e^{j\phi_j}$, a_j = -0.5, φ_j = 165, 175, 179
Antenna gain (dB)		$G_{aj} = 6$
Amplifier gain (dB)		$G_j = 70$
Baseline distance (m)		$d_c = 10$
Rotation angle (degrees)		$\theta_c = 30$
Antenna 1	Range (m)	$R_1 = 1002.5$
	Angle (degrees)	$\theta_1 = 0.2481$, $\varphi_1 = 0$
Antenna 2	Range (m)	$R_2 = 997.5$
	Angle (degrees)	$\theta_2 = -0.2481$, $\varphi_2 = 0$

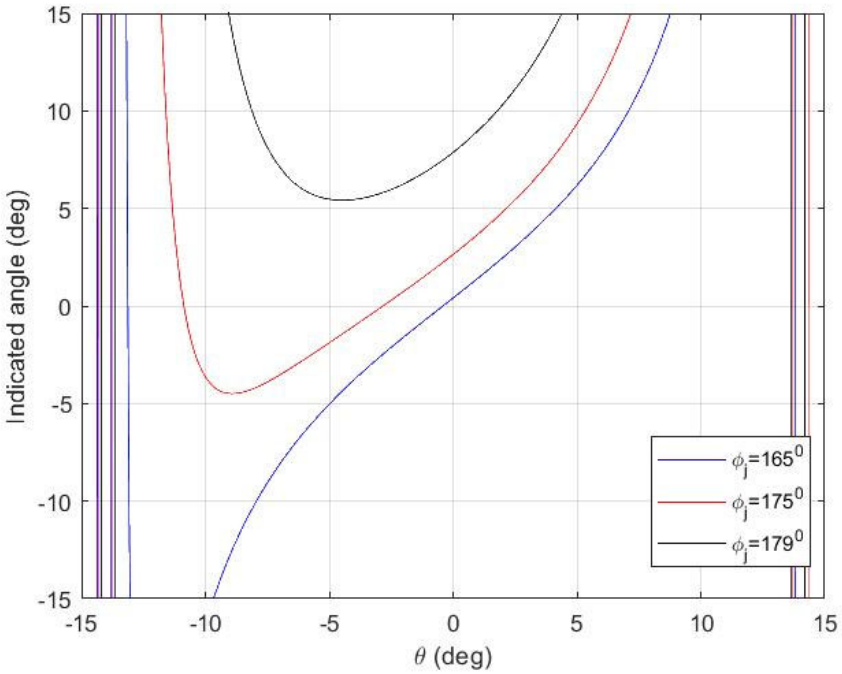

Figure 17. Indicated angles for three different φ_j using the antenna parameters described in Section II

Table 6. Results of Simulations 1 and 2

Simulation	φ_j (degrees)	Angle errors (degrees)
From [9]	165	0.67 (validation)
1	165	0.2704
2	165	0.4081
From [9]	175	2.67 (validation)
1	175	1.9959
2	175	2.6328
From [9]	179	6 (validation)
1	179	6.7076
2	179	7.8670

B. SIMULATIONS AND RESULTS CONCERNING CROSS-EYE JAMMING

As presented in this section, simulations were performed that concern the technique of cross-eye jamming in general. The parameters used in these simulations, unless otherwise noted, are shown in Table 7.

Table 7. Parameters used in Sections IIIB and IIIC

Radar		
Parameter		Symbol and value
Transmit power (W)		$P_t = 1$
Frequency (MHz)		$f = 300$
Sum beam gain (dB)		$G_s = 16.93$
Sum beam relative sidelobe level (dB)		$sll_s = 20$
Difference beam gain (dB)		$G_d = 14.68$
Difference beam relative sidelobe level (dB)		$sll_d = 20$
Number of elements		$N = 10$
Spacing between elements (m)		$d_x = 0.5$
Target		
Parameter		Symbol and value
Range (m)		$R_t = 1000$
Direction (degrees)		$\theta_t = 0$, $\varphi_t = 0$
RCS (m^2)		$\sigma \cdot e^{j\phi_\sigma} = 1$
Jammer		
Parameter		Symbol and value
Cross-eye weight (dB, degrees)		$\alpha_j e^{j\phi_j}$, a_j = -0.5, $\varphi_j = 175$
Antenna gain (dB)		$G_{aj} = 6$
Amplifier gain (dB)		$G_j = 60$
Baseline distance (m)		$d_c = 10$
Rotation angle (degrees)		$\theta_c = 0$
Antenna 1	Range (m)	$R_1 = 1000$
	Angle (degrees)	$\theta_1 = 0.2865$, $\varphi_1 = 0$
Antenna 2	Range (m)	$R_2 = 1000$
	Angle (degrees)	$\theta_2 = -0.2865$, $\varphi_2 = 0$

1. Simulation Regarding Jammer-To-Signal Ratio (JSR)

Simulation 3 was performed to examine the effect of the jammer-to-signal ratio (JSR) on the angle error. All the parameters remained constant except for the gain of the amplifier of the jammer G_j and the phase difference between the two jammer antennas φ_j. The cases examined were with four different φ_j values: 165°, 170°, 175°, and 179°. The rest of the parameters are shown in Table 7, and the results are shown in Figure 18. An interesting outcome is that for a large JSR (higher than 50 dB), the angle error becomes independent of the JSR. Another observation worth mentioning is that if φ_j is less than 175° (or greater than 185°), the maximum angle error occurs at a certain JSR, and if the JSR increases further, the angle error decreases.

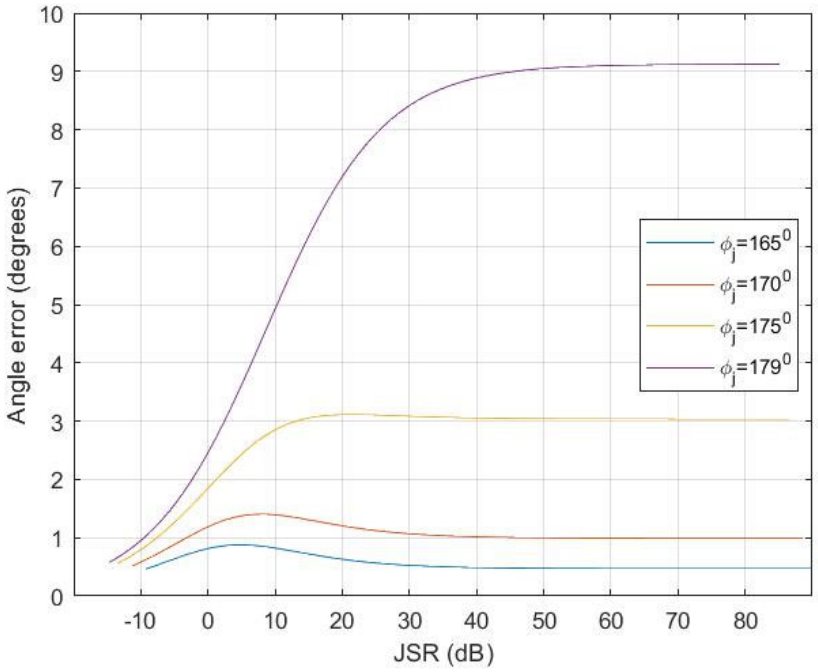

Figure 18. Angle error versus JSR for Simulation 3

2. Simulation Regarding the Distance of the Target and Jammer

In this part, the effectiveness of cross-eye jamming was examined when a target with a jammer approached the radar (Simulation 4). The jammer was at the same distance

as the target with respect to the radar, and in both cases, hardwired (classical retrodirective implementation) and wireless (UAVs as platforms) simulations were performed. The parameters are shown in Table 7, except for the distance of the target and the jammer, which was a variable. The angle error versus the distance plot is shown in Figure 19 and agrees with the observation of [21] that a cross-eye jammer creates a constant angular bias, not just an angular error. Also, the plot shows that the angle error is inversely proportional to the distance, which agrees with [18], as derived in chapter 2 of [3].

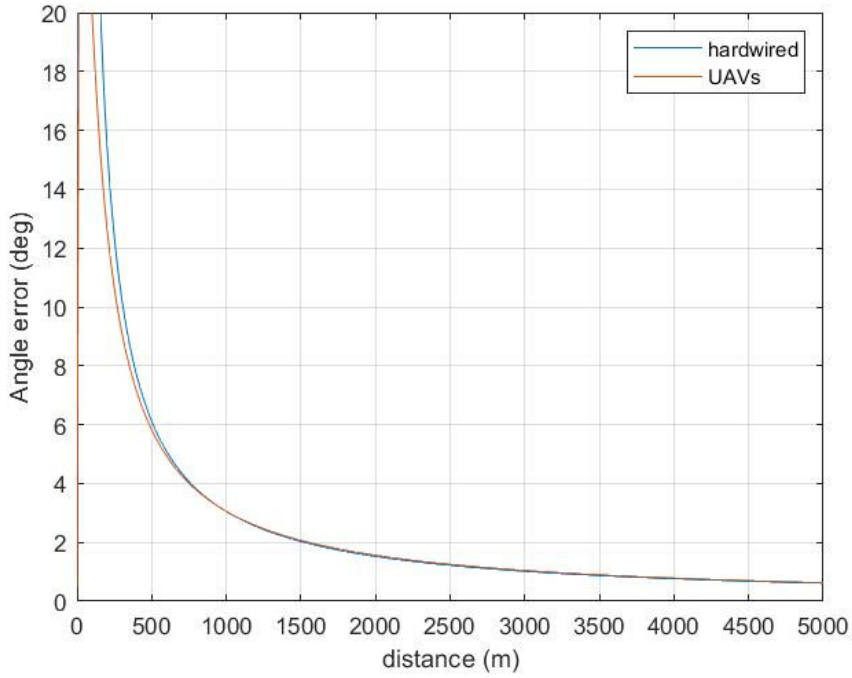

Figure 19. Angle error versus the distance between the radar and target and the jammer for Simulation 4

3. Simulations Regarding the Amplitude (a_j) and Phase Difference (φ_j) between the Jammer Antennas

The relative amplitude (a_j) and phase difference (φ_j) were examined one at a time and both together. The parameters remained the same as shown in Table 7. The angle error versus the relative amplitude is shown in Figure 20 (Simulation 5). The maximum angle error was achieved near the matched amplitudes whereas, at exactly matched amplitudes,

the angle error diminished because the two signals from the jammer antennas cancelled each other. The cases between the hardwired and UAVs were slightly different. The plot was shifted to the right for the wireless case. This was a result of a lower JSR in the wireless case than in the wired case, as shown in Figure 21. To have a better view of this phenomenon, in Figure 22, the angle error versus the relative amplitude for various jammer amplifier gains is shown, and in Figure 23, the JSR versus the relative amplitude is shown. As the JSR is reduced, the plots shift to the right, and the maximum angle errors are reduced, which agrees with [2], [4].

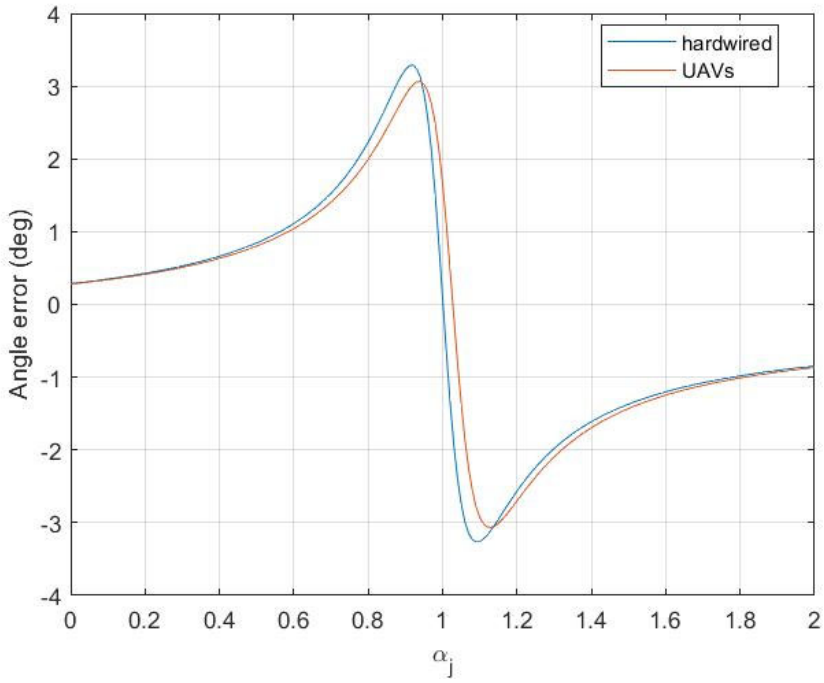

Figure 20. Angle error versus the relative amplitude between the two jammer signals

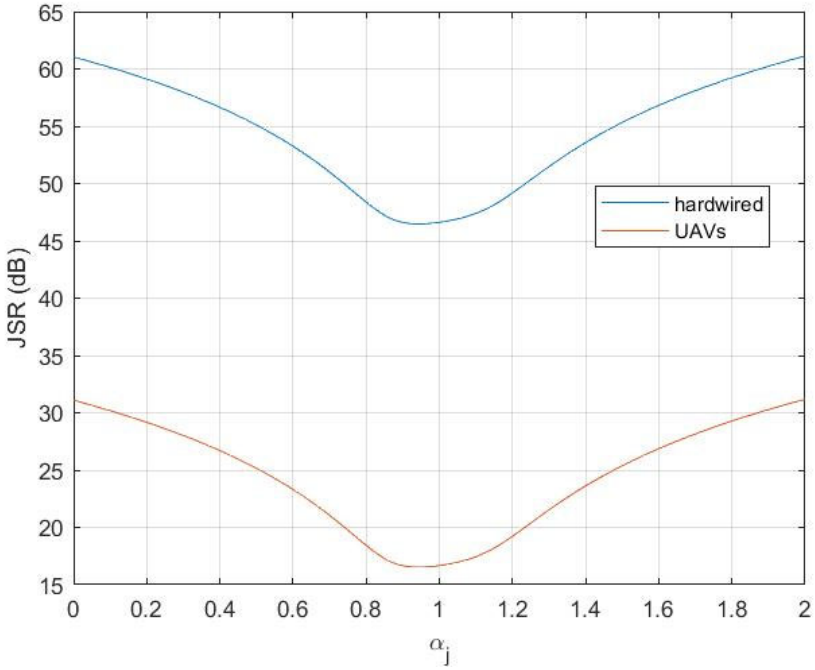

Figure 21. JSR versus the relative amplitude between the two jammer signals

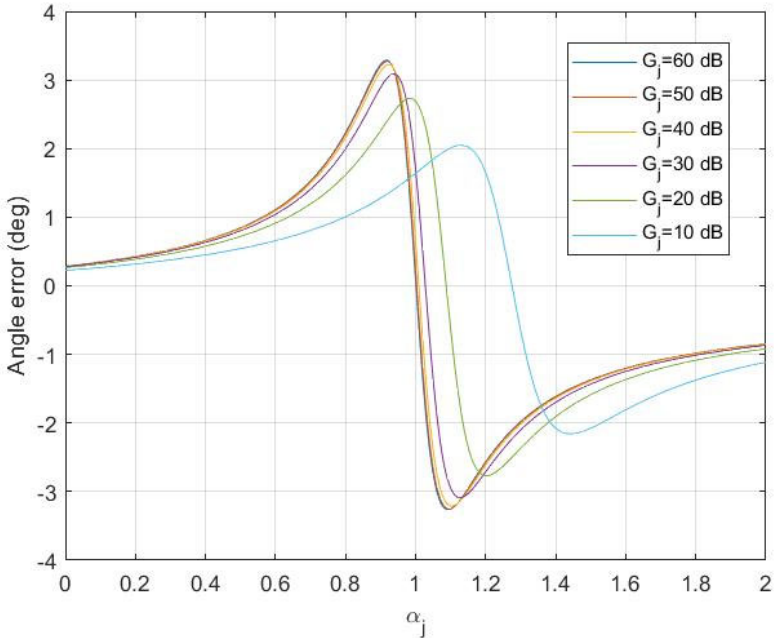

Figure 22. Angle error versus the relative amplitude between the two jammer signals for different jammer amplifier gains

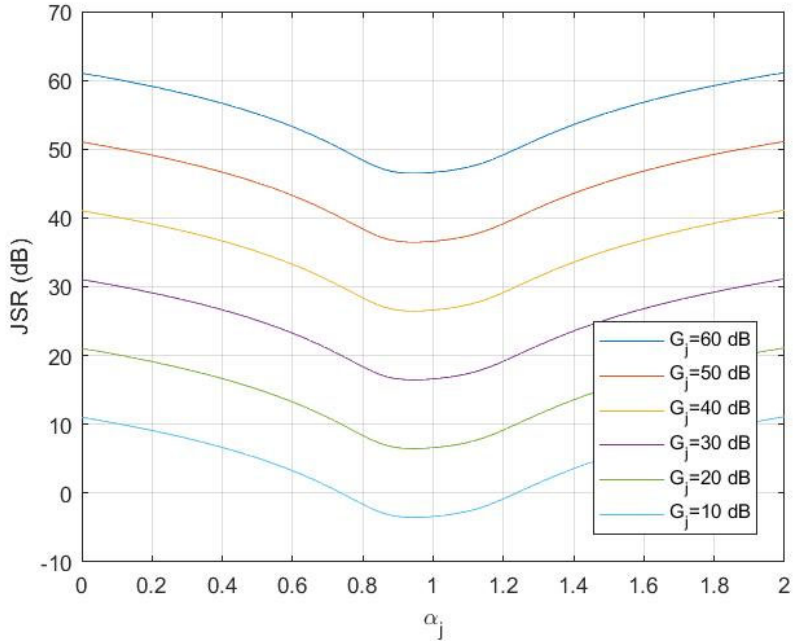

Figure 23. JSR versus the relative amplitude between the two jammer signals for different jammer amplifier gains

Next, the phase difference between the two jammer signals became the variable and the relative amplitude remained constant (Simulation 6). The results in Figure 24 are as expected since the maximum angle error occurs at 180°. The JSR is plotted in Figure 25; the minimum occurs when the phase difference is 180°. To see the effect of JSR in this simulation, the same plot with different jammer amplifier gains is shown in Figure 26 and the resulting JSR in Figure 27. From Figure 26, we can conclude that as the JSR increases, the angle error also increases because $174° < \varphi_j < 186°$, whereas out of this range, the opposite happens.

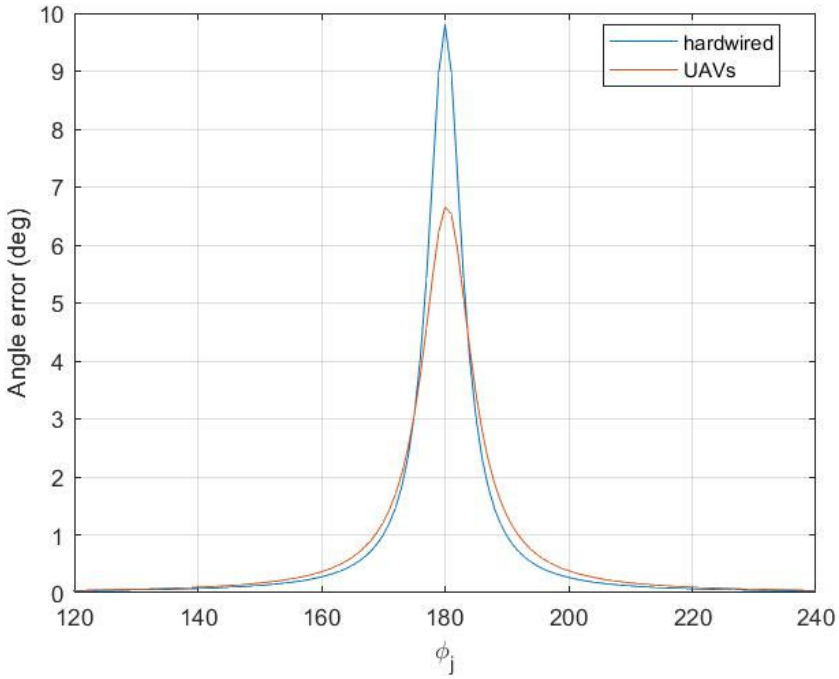

Figure 24. Angle error versus the phase difference between the two jammer signals

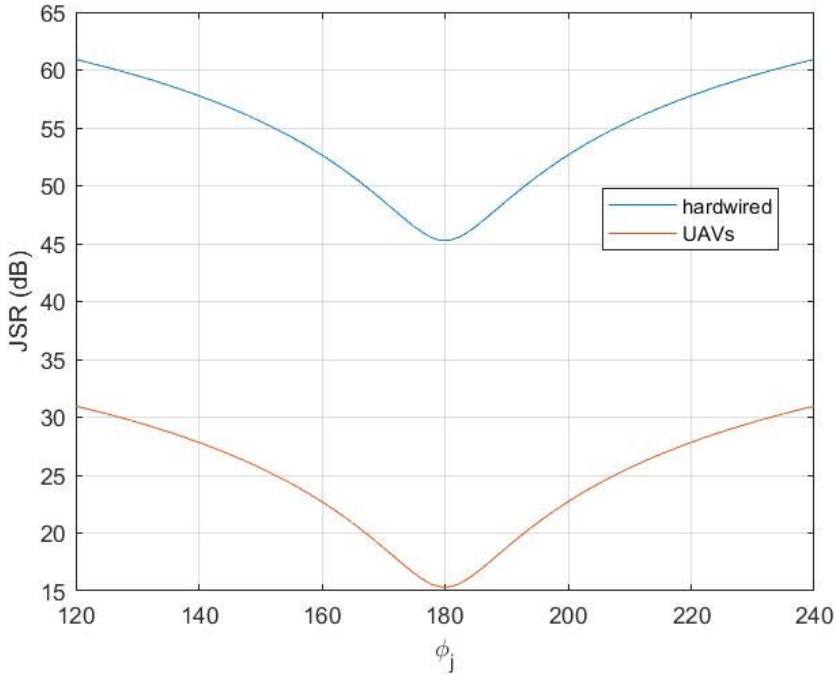

Figure 25. JSR versus the phase difference between the two jammer signals

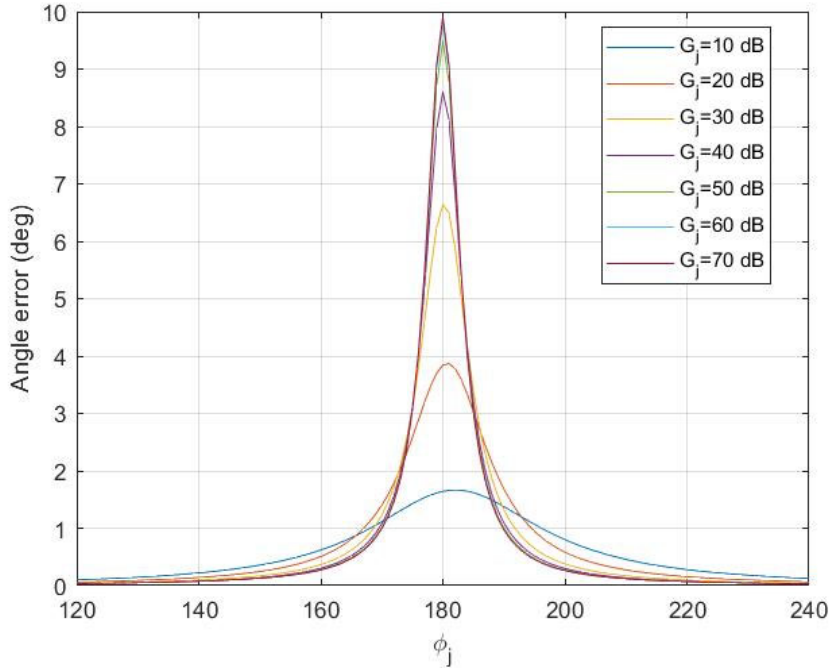

Figure 26. Angle error versus the phase difference between the two jammer signals for various jammer amplifier gains

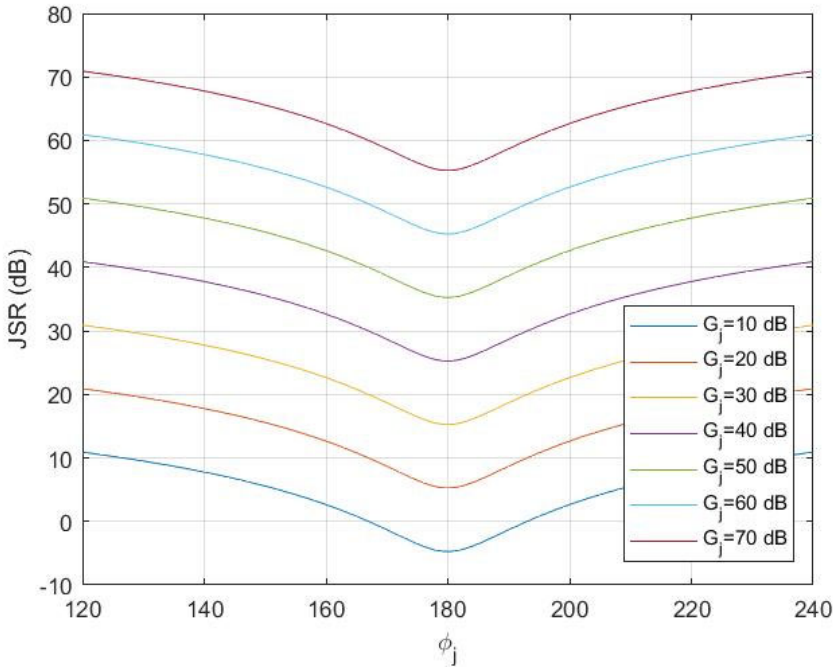

Figure 27. JSR versus the phase difference between the two jammer signals for various jammer amplifier gains

Since the relative amplitude (a_j) and phase difference (φ_j) were examined separately, in Simulation 7, both were varied, and the angle error was plotted as contours. The angle error versus the two variables is depicted in Figure 28 for the hardwired case and in Figure 29 for the wireless case. The JSR fluctuates for the different variable values from 47 to 52 dB for the wired case and from 17 to 22 dB for the UAVs; the JSR plot of the wired case is shown in Figure 30. The maximum angle error is produced when the relative amplitude is matched, and the phase difference is 180° for the hardwired case. For the wireless case, due to the low JSR, the maximum angle error is accomplished when the relative amplitude is 0.2 dB and the phase difference is 180°, which agree with the previous results and [2], [4].

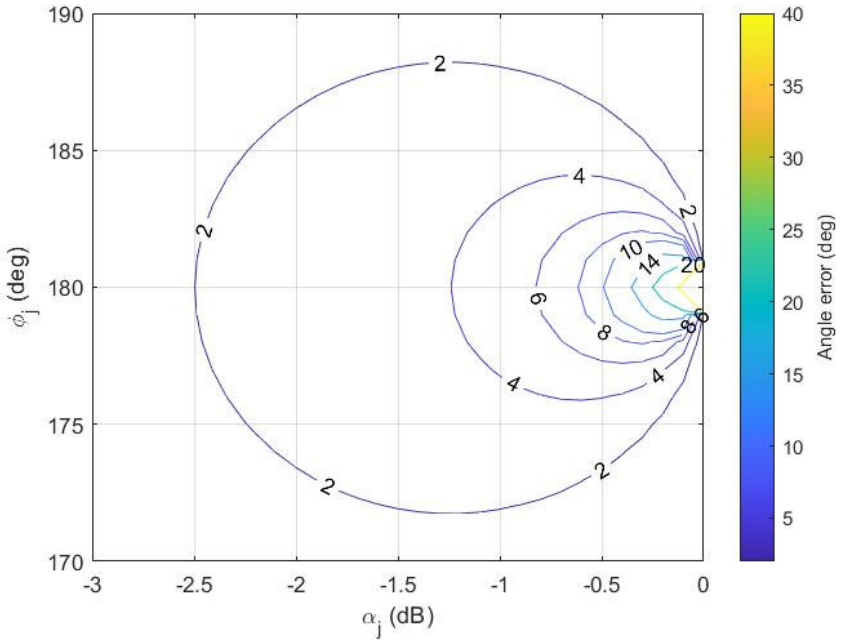

Figure 28. Angle error versus the relative amplitude and the phase difference between the two jammer signals for the hardwired case

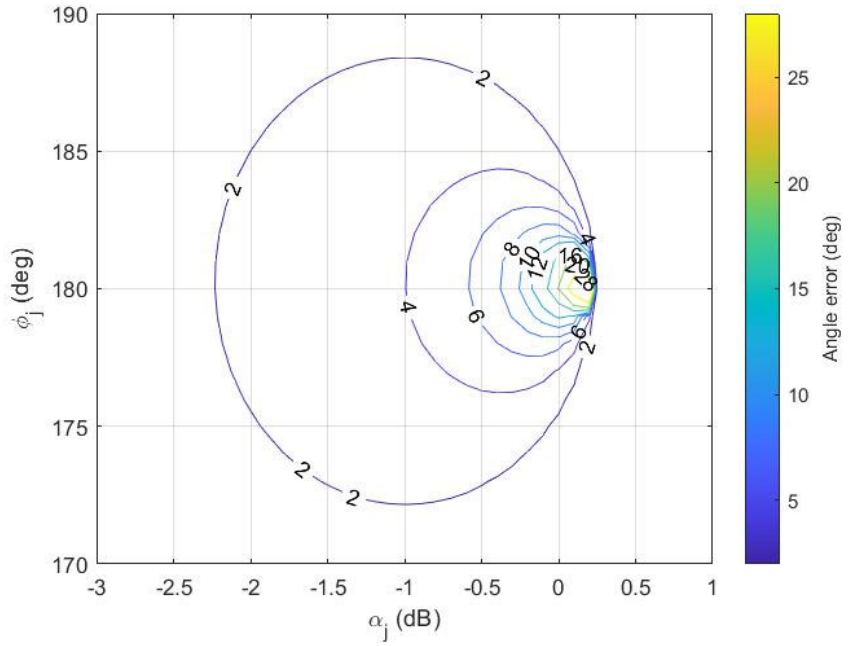

Figure 29. Angle error versus the relative amplitude and phase difference between the two jammer signals for the wireless case

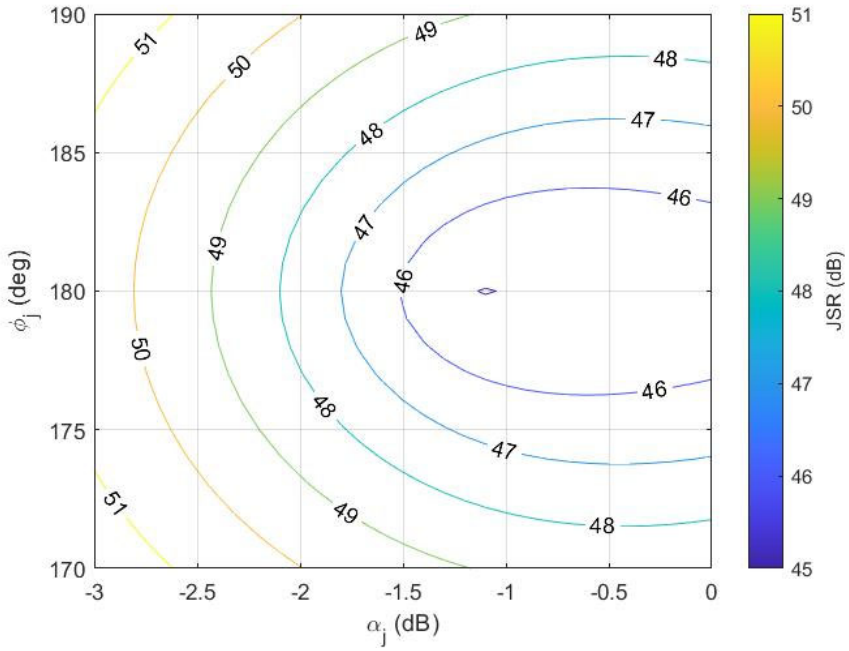

Figure 30. JSR versus the relative amplitude and phase difference between the two jammer signals for the hardwired case

C. SIMULATIONS AND RESULTS CONCERNING THE USE OF UAVS IN CROSS-EYE JAMMING

1. Simulation Regarding the Rotation Angle (θ_c)

The rotation angle (θ_c) was allowed to change in Simulation 8. The UAVs remained fixed at their best performance position because they could move independently while the target could rotate 360°. The rest of the parameters remained the same as in Table 7. The result is shown in Figure 31. The use of the UAVs can eliminate the negative effect that the rotation angle causes to the cross-eye efficiency.

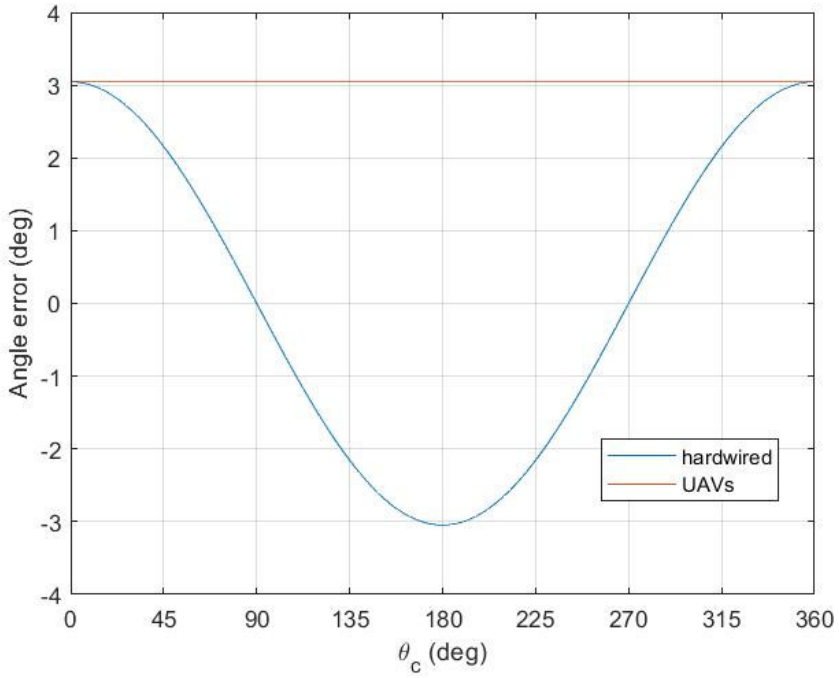

Figure 31. Angle error versus the rotation angle (θ_c)

2. Simulation Regarding the Spacing between the Jammer Antennas (d_c)

In Simulation 9, the distance between the jammer antennas (d_c) became the variable. The distance of the UAVs increased from 10 m to 200 m while the distance of the hardwired jammer antennas remained fixed at 10 m. The rest of the parameters remained the same as in Table 7. The result is shown in Figures 32 and 33. The dashed line is the

negative value of the angle error caused by the jammer with the hardwired antennas. This line was added to help the reader understand when the angle error produced by the wireless case was larger than the hardwired case. Large angle errors could be produced with the use of the UAVs although there were areas where the angle error was smaller than the hardwired case. The phase of the signals from the UAVs relative to the target echo phase were changing, thus by adding constructively or destructively. As shown in Figure 33, the portion of the graph in which the angle error is smaller than the hardwired case is very small, as the slope at this range is almost vertical.

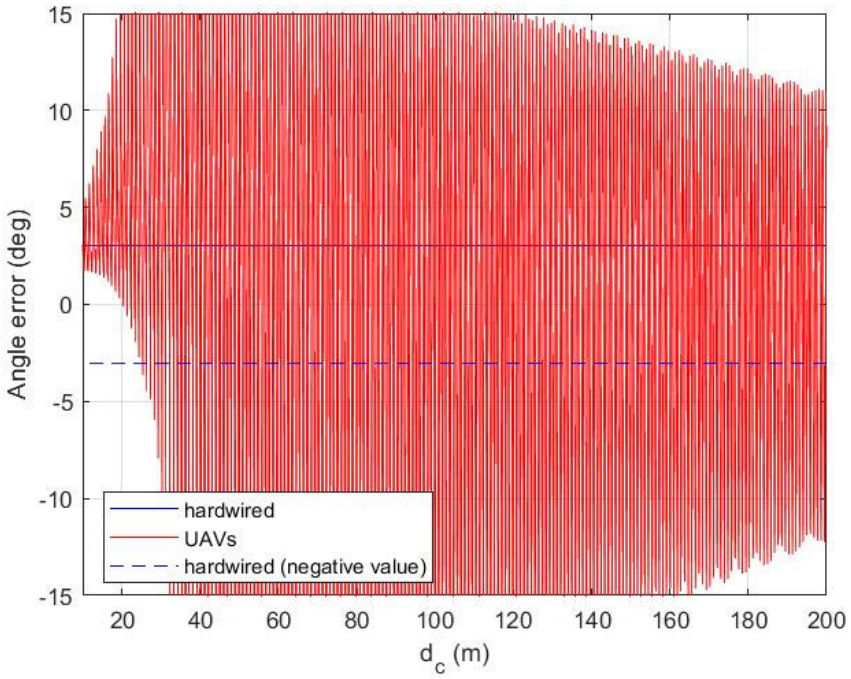

Figure 32. Angle error versus the distance between the jammer antennas (d_c)

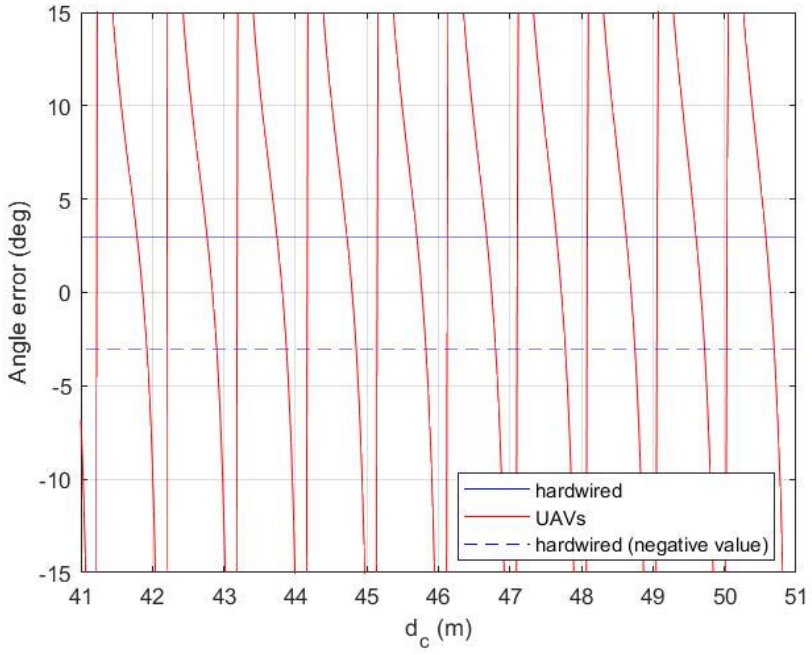

Figure 33. Angle error versus the distance between the jammer antennas (d_c), scale expanded

3. Simulation Regarding the Distance between the Jammer Antennas and the Radar (R_1, R_2)

For this part, Simulation 10 was performed with the target stationed at 1,000 m as the UAVs approached the radar. The distance (d_c) between the UAVs remained 10 m and the rotation angle (θ_c) was 0° for the duration of the simulation. The rest of the parameters are given in Table 7. The result is shown in Figures 34 and 35. The use of the UAVs can produce larger errors than the hardwired case. If the UAVs are positioned half the target distance from the radar, the angle error is doubled, which is a significant accomplishment. The angle error caused by the UAVs has a 3° fluctuation near the target (at 1000 m), which gradually decreases as the UAVs approach the radar. This occurs because the distance that the signals of the wireless jammer travel changes constantly, causing a phase difference with respect to the return signal from the target. From Figure 35, we can derive that the sinusoid repeats every 0.5 m, which is equal to half a wavelength.

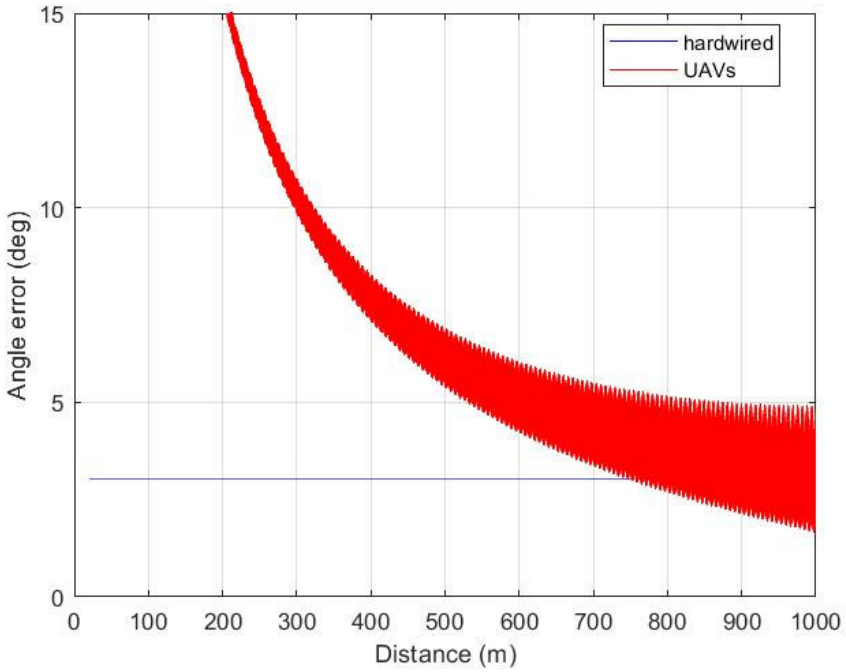

Figure 34. Angle error versus the distance of the UAVs with respect to the radar

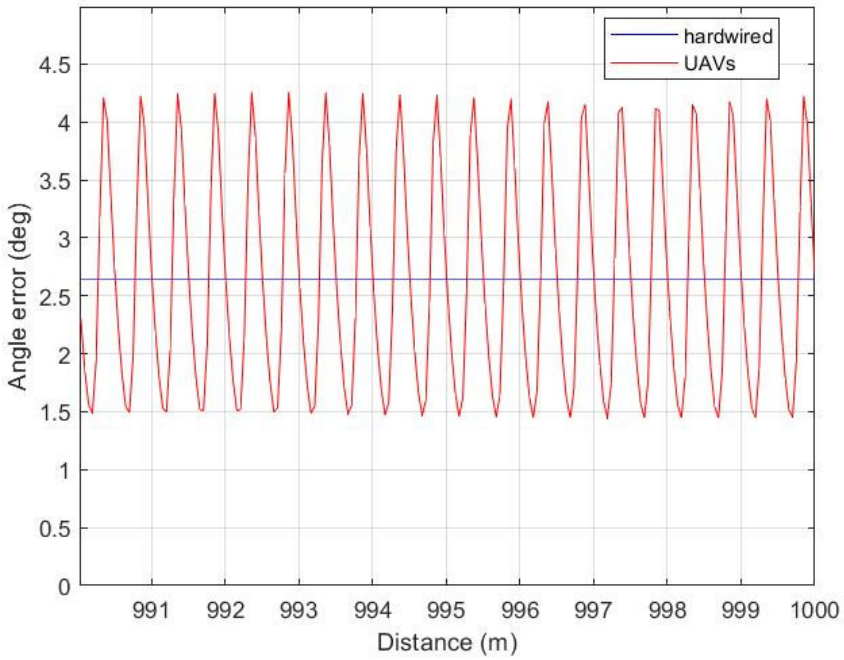

Figure 35. Angle error versus the distance of the UAVs with respect to the radar, scale expanded

D. CHAPTER SUMMARY

This chapter presented MATLAB simulations that tested the effectiveness of the proposed UAV implementation of a cross-eye jammer. The simulations are summarized in Table 8. The results show that the use of UAVs as jammer antenna platforms can be very effective and induce large angle errors, which cannot be produced with the original hardwired implementation. The advantage of positioning the UAVs closer to the radar with zero rotation angle can make this method more efficient than the original implementation. However, the distance between the UAVs should be selected carefully because some distances can cause smaller angle errors than the original implementation. This will be difficult to do at high frequencies where the wavelength is small. To conclude, the use of UAVs with a known enemy direction can induce angle errors, which the original hardwired implementation cannot, making cross-eye jamming a powerful EA method against monopulse radars.

Table 8. Summary of simulations

Simulation	Objective	Result
1	Verify results with [3], [9].	The results are similar.
2	Verify results with [3], [9].	The results are similar.
3	Vary the JSR.	After a certain JSR, the angle error becomes independent of the JSR.
4	Vary the distance between the target and the radar.	The angle error is inversely proportional to the distance.
5	Vary the relative amplitude (α_j).	The maximum angle error occurs at almost matched amplitudes.
6	Vary the phase difference between the two jammer signals (φ_j).	The maximum angle error occurs at phase difference equal to 180°.
7	Vary both the relative amplitude (α_j) and the phase difference between the two jammer signals (φ_j).	The maximum angle error occurs at matched amplitudes and phase difference equal to 180°.
8	Vary the rotation angle (θ_c) for the hardwired implementation, while the UAVs remain fixed.	The use of the UAVs can eliminate the negative effect that the rotation angle causes to the cross-eye efficiency.
9	Vary the distance between the jammer antennas.	Large angle errors can be produced with the use of the UAVs, although oscillations occur due to the change of the jammer signals phase.
10	Vary the distance between the UAVs and the radar, while the target remains fixed at 1,000 m.	Large angle errors can be produced with the use of the UAVs (at half the distance, the angle error is doubled).

THIS PAGE INTENTIONALLY LEFT BLANK

IV. CONCLUSION AND RECOMMENDATIONS

A. SUMMARY AND CONCLUSIONS

The objective of this thesis was to examine cross-eye jamming and the use of UAVs as cross-eye jammer antenna platforms. A MATLAB script simulating an environment with a radar, a target, and a cross-eye jammer was created. Specifically, a phased array was used as a monopulse antenna, and the jammer was a retrodirective two-element cross-eye jammer whose elements were installed on two UAVs. Also, to compare the results with the original retrodirective hardwired implementation, a reference cross-eye jammer was simulated at the wingtips of the target.

At this point, it is wise to remind the reader that for the approach of using UAVs as jammer platforms to be effective, the return of the target and the signals from the jammer should be synchronized and arrive at the same time at the radar. This may require introducing delay in the jammer signals if they operate at a shorter range than the target.

The results of the simulations are very encouraging since large angle errors can be induced in the hostile radar with the use of UAVs. There is freedom to place the UAVs wherever necessary to make cross-eye jamming even more efficient. The negative effect that the rotation angle causes on the efficiency of the jammer is eliminated. Furthermore, if the UAVs are stationed at a small distance ahead of the target for tactical or other reasons, very large errors could be produced. For deployment, the only restriction is to know the direction of the threat, station the UAVs accordingly, and synchronize the signals at this direction. From a tactical perspective in a multi-threat environment, if the UAVs are close to the target, they could easily be stationed accordingly to face a threat from a different direction from the initial threat.

To sum up, after examining the use of UAVs as cross-eye jammer platforms, we can say that the results are promising. Given the environment in which EW techniques are developing rapidly, this approach could contribute to the effectiveness of the cross-eye jamming technique and the overall goal of spectrum dominance.

B. FUTURE WORK

An investigation of the use of UAVs as cross-eye jammer platforms was made. However, this approach needs to be further investigated to examine all parameters thoroughly. The effect of the parameters on the efficiency of the wireless implementation should be studied more as unexpected results may occur. The positions of the UAVs that maximize the angle error vary depending on the parameters. The way to find these positions should be found.

Furthermore, the oscillations observed in Simulations 9 and 10 result in a quick and significant change of the angle error induced in the radar, especially at high frequencies. The oscillations are due to the interference effects between the target echo and the jammer signals, and they would not occur if the target RCS was much larger or much smaller. The effect of the oscillations on radar performance will depend on the radar parameters (e.g., pulse width or pulse repetition frequency). This could affect the efficiency of the radar and cause the radar to lose tracking of the target more easily than expected. These effects should be examined and verified.

Finally, the tolerances on the synchronization of the jammer signals and the target echo need to be examined. The distances between the target, the first UAV, and the second, as well as the direction of the hostile radar, determine the delay that should be applied to the jammers. The precision of those measurements and the radar's range resolution would determine whether the wireless implementation could be effective under real conditions.

LIST OF REFERENCES

[1] M. I. Skolnik, "Tracking radar," in *Introduction to Radar Systems*, 3rd ed., McGraw-Hill Higher Education, 2001, pp. 210–275.

[2] W. P. du Plessis, "Practical implications of recent cross-eye jamming research," *Counc. Sci. Ind. Res.*, pp. 167–174, Sep. 2012.

[3] W. P. du Plessis, "A comprehensive investigation of retrodirective cross-eye jamming," Ph.D. dissertation, Dept. of Electrical, Electronic and Computer Engineering, University of Pretoria, South Africa, 2010.

[4] W. P. du Plessis, "Platform skin return and retrodirective cross-eye jamming," *IEEE Trans. Aerosp. Electron. Syst.*, vol. 48, no. 1, pp. 490–501, Jan. 2012.

[5] T. Liu, D. Liao, X. Wei, and L. Li, "Performance analysis of multiple-element retrodirective cross-eye jamming based on linear array," *IEEE Trans. Aerosp. Electron. Syst.*, vol. 51, no. 3, Jan. 2015. [Online]. doi: 10.1109/TAES.2015.140035.

[6] N. Levanon, "Monopulse antenna tracking," in *Radar Principles*, 1st ed., John Wiley & sons, 1988, pp. 285–301.

[7] D. C. Jenn, "Complex targets," in *Radar and Laser Cross Section Engineering*, 2nd ed., AIAA, 2005, pp. 257–333.

[8] D. Adamy, "Cross eye jamming," in *EW 101: A First Course in Electronic Warfare*, Artech House, 2001, pp. 220–222.

[9] W. P. du Plessis, J. W. Odendaal, and J. Joubert, "Extended analysis of retrodirective cross-eye jamming," *IEEE Trans. Antennas Propag.*, vol. 57, no. 9, pp. 2803–2806, Sep. 2009.

[10] "Loyal Wingman," Boeing, Apr. 30, 2021. [Online]. Available: http://www.boeing.com/defense/airpower-teaming-system/

[11] T. W. Tucker and B. Vidger, "Cross-eye jamming effectiveness," Tactical Technol., 2009. [Online]. Available: http://www.tti-ecm.com

[12] D. C. Jenn, "notes for EC4610 Microwave Devices and Radar."

[13] L. Falk, "Cross-eye jamming of monopulse radar," *IEEE Waveform Divers. Des.*, pp. 209–213, 2007.

[14] N. M. Harwood, W. N. Dawber, V. A. Kluckers, and G. E. James, "Multiple-element crosseye," *IET Radar Sonar Navig.*, vol. 1, no. 1, Feb. 2007.

[15] S. Liu, C. Dong, J. Xu, G. Zhao, and Y. Zhu, “Analysis of rotating cross-eye jamming,” *IEEE Antennas Wirel. Propag. Lett.*, vol. 14, pp. 939–942, 2015.

[16] R. H. Delano, “A theory of target glint or angular scintillation in radar tracking,” *Proc. IRE*, vol. 41, no. 12, pp. 1778–1784, Dec. 1953.

[17] J. E. Meade, “Target considerations,” in *Principles of Guided Missile Design*, D. Van Nostrand Company, 1955, pp. 435–444.

[18] S. M. Sherman, “Complex indicated angles applied to unresolved radar targets and multipath,” *IEEE Trans. Aerosp. Electron. Syst.*, vol. 7, no. 1, pp. 160–170, Jan. 1971.

[19] D. C. Schleher, “EA against modern radar systems,” in *Electronic Warfare in the Information Age*, Norwood, MA: Artech House, 1999, pp. 201–292.

[20] S. A. Vakin and L. N. Shustov, “Principles of jamming and electronic reconnaissance,” vol. 1, U.S. Air Force, Tech. FTD-MT-24-115-69, 1969.

[21] P. E. Redmill, “The principles of artificial glint jamming (‘cross eye’),” Ministry of Aviation, Royal Aircraft Establishment (Fanborough), Tech. Note RAD. 831 AD336943L, Mar. 1963.

[22] J. E. Lindsay, “Angular glint and the moving, rotating, complex radar target,” *IEEE Trans. Aerosp. Electron. Syst.*, vol. 4, no. 2, pp. 164–173, Mar. 1968.

[23] J. H. Dunn and D. D. Howard, “Radar target amplitude, angle, and doppler scintillation from analysis of the echo signal propagating in space,” *IEEE Trans. Microw. Theory Tech.*, vol. 16, no. 9, pp. 715–728, Sep. 1968.

[24] A. I. Leonov and K. I. Fomichev, *Monopulse radar*. Fairborn, OH: Foreign Technology Div., Wright-Patterson Air Force Base, 1970.

[25] W. P. du Plessis, “Phase-conjugating retrodirective cross-eye jamming,” *Electron. Lett.*, vol. 56, no. 20, pp. 1079–1082, Sep. 2020.

[26] W. L. Stutzman and G. A. Thiele, *Antenna theory and design*, 3rd ed. John Wiley & Sons, 2013.

INITIAL DISTRIBUTION LIST

1. Defense Technical Information Center
   Ft. Belvoir, Virginia

2. Dudley Knox Library
   Naval Postgraduate School
   Monterey, California